PNAS

Supplementary Information for

5-methylcytosine (m^5C) RNA modification controls the innate immune response to virus infection by regulating type I interferons

Yuexiu Zhang[a,1], Li-Sheng Zhang[b,c,d,1], Qing Dai[b,c,d], Phylip Chen[f], Mijia Lu[a], Elizabeth L Kairis[a], Valarmathy Murugaiah[a], Jiayu Xu[a], Rajni Kant Shukla[a], Xueya Liang[a], Zhongyu Zou[b,c,d], Estelle Cormet-Boyaka[a], Jianming Qiu[g], Mark E. Peeples[f, h], Amit Sharma[a,i], Chuan He[b,c,d,e,2], Jianrong Li[a,2]

[a]Department of Veterinary Biosciences, College of Veterinary Medicine, The Ohio State University, Columbus, OH, 43210;
[b]Department of Chemistry, The University of Chicago, Chicago, IL 60637;
[c]Department of Biochemistry and Molecular Biology, The University of Chicago, Chicago, IL 60637;
[d]Institute for Biophysical Dynamics, The University of Chicago, Chicago, IL 60637;
[e]Howard Hughes Medical Institute, The University of Chicago, Chicago, IL 60637;
[f]Center for Vaccines and Immunity, Abigail Wexner Research Institute, Nationwide Children's Hospital, Columbus, OH 43205;
[g]Department of Microbiology, Molecular Genetics and Immunology, University of Kansas Medical Center, Kansas City, KS; 66160
[h]Department of Pediatrics, College of Medicine, The Ohio State University, Columbus, OH 43205;
[i]Department of Microbial Infection and Immunity, College of Medicine, The Ohio State University, Columbus, OH, 43210

[1]These authors contribute equally to this work.
[2]Co-Corresponding authors
Email: li.926@osu.edu; chuanhe@uchicago.edu.

This PDF file includes:

Supplementary Materials and Methods

Cell culture. A549 (ATCC CCL-185), Vero (ATCC CRLCCL81), Vero E6 cells (ATCC CRL-1586), HEp-2 (ATCC CCL-23), and THP-1 (TIB-202™) cells were purchased from the American Type Culture Collection and were maintained in DMEM supplemented with 10% fetal bovine serum (FBS). Wild type A549-Dual, RIG-I knockout A549 cells (A549-Dual KO-RIG-I), and MDA5 knockout A549 cells (A549-Dual KO-MDA5) were purchased from InvivoGen, and were maintained in DMEM supplemented with 10% FBS, Normocin (100 $\mu g\,ml^{-1}$), blasticidin (10 $\mu g\,ml^{-1}$) and zeocin (100 $\mu g\,ml^{-1}$). All cells were cultured at 37°C with 5% CO_2. All cell lines used in this study were free of mycoplasma, as confirmed by the LookOut Mycoplasma PCR Detection Kit (Sigma). Cell lines were authenticated by the ATCC or InvivoGen.

Animals. 6-week-old specific pathogen free (SPF) female C57BL/6J mice were purchased from Jackson Laboratory. Three female and two male heterozygous NSUN2 knockout mice ($NSUN2^{+/-}$) with B6CBAF1/J genetic background were generously provided by Dr. Michaela Frye at German Cancer Research Center (Heidelberg, Germany) (1, 2). Detailed genotyping method for NSUN2 knockout mice was described previously (1). A PCR-based strategy was used to distinguish the wild-type and NSUN2 gene trap alleles. The primers SR2 (5′-GCC AAA CCT ACA GGT GGG GTC TTT) and B34 (5′- TGT AAA ACG ACG GGA TCC GCC) were used to amplify a fragment 650 bp of the β-geo cassette. The primers Misu-Int8-5′ (5′-AAG TAA GGC ATA GTA ACA GCT AC) and Misu-Int8-3′ (5′-AGG GAG GGT CTG GAA AGA TG) were used to amplify a fragment of 322 bp of the wild-type allele. The animal study was conducted in strict accordance with USDA regulations and the recommendations in the Guide for the Care and

Use of Laboratory Animals of the National Research Council and was approved by The Ohio State University Institutional Animal Care and Use Committee (IACUC; animal protocol no. 2009A0160-R3). The animals were housed within the University Laboratory Animal Resources (ULAR) facilities of The Ohio State University according to the guidelines of the Institutional Animal Care and Use Committee (IACUC). The animal care facilities at The Ohio State University are AAALAC accredited. Every effort was made to minimize potential distress, pain, or discomfort to the animals throughout all experiments.

Virus stocks. Recombinant human respiratory syncytial virus (RSV) A2 strain expressing GFP (rgRSV), vesicular stomatitis virus (VSV) Indiana strain expressing GFP (rVSV-GFP), human metapneumovirus (hMPV) NL/1/00 strain were grown in A549 cells. Sendai virus expressing GFP (rSeV-GFP) and herpes simplex virus 1 expressing GFP (rHSV1-GFP) were grown in Vero-CCL81 cells. HIV-1 was grown THP-1 cells. Viral titers were determined by plaque assay or $TCID_{50}$ assay.

Drugs and reagents. The Pol III inhibitor ML-60218 was purchased from Calbiochem (San Diego, CA) and was dissolved in DMSO to 10 mM as stock solution. MTT assay kit was purchased from Abcam (ab211091).

Antibodies. The antibodies used in this study includes anti-NSUN2 antibody (1:2000, Proteintech), anti-RSV serum (1:400, Virostat, Westbrook, ME), anti-RSV F (1:3000, Abcam), anti-β-Actin (1:5000, Proteintech), anti-hMPV serum (1:2000, prepared in cotton rats), anti-hMPV N antibody (1:2000, US Biological), anti-VSV G antibody(1:5000, Kerafast), anti-VSV N antibody (1:2000,

Kerafast), anti-RIG-I (Abcam, ab180675), anti-MDA5 (Abcam, ab79055), anti-IRF3 (Phospho S386) (Abcam, ab76493), anti-YBX1 (1:1000, Proteintech, 20339-1-AP), anti-ALYREF (1:1000, Abcam, ab6141), anti-SRP9 (1:1000, Proteintech, 11195-1-AP), anti-SRP14 (1:1000, Proteintech, 11528-1-AP), and anti-FLAG (Sigma-Aldrich).

Plasmids and site-directed mutagenesis. Plasmid pCAGGS encoding NSUN2 were synthesized by IDT. Alanine mutations to C271 and C321 in NSUN2 were introduced into the plasmid pCAGGS-NUSN2 using QuikChange site-directed mutagenesis kit (Stratagene). The plasmids pGFH-9 (Addgene plasmid # 39538) and pGFH-14c (Addgene plasmid # 39541) are gifts from Dr. Katharina Strub (Addgene plasmid # 39538; http://n2t.net/addgene:39538; RRID: Addgene 39538)(3). All constructs were sequenced at The Ohio State University Plant Microbe Genetics Facility.

siRNAs and plasmid transfection. The siRNAs used in this study include siRNAs for knockdown of NSUN2 (OriGene, SR324319), MDA5 (siGENOME SMARTpool, M-013041-00-0010), 7SLRNA (Qiagen, NR002715), RPPH1 (Qiagen, NR002312), siYBX1 (siGENOME SMARTpool, M-010213-03-0005), siALYREF (siGENOME SMARTpool, M-012078-01-0005), and non-targeting control siRNA (siNC). All siRNA and plasmid transfections were performed using the Lipofectamine 3000 transfection reagent (ThermoFisher) according to the manufacturer's instructions. In brief, 90% confluent A549 cells in 24-well plates were transfected with 1 μg of plasmid or 12-24 nM of siRNA, followed by virus infection. In some cases, cells were transfected with two rounds siRNA with 24 h interval. At indicated time points, cells were lysed in RIPA

buffer (Abcam) on ice and collected for Western blot, or total RNA was extracted from cells for real-time PCR.

Generation of NSUN2 knockout A4549 and THP-1 **cell line.** CRISPR-Cas9 was used to knock out the NSUN2 gene in A549 and THP-1 cells. Three single guide RNAs (sgRNAs) specific for exon 4 of the NSUN2 gene (sgRNA1, 5'-UUCCUUCCUCAGGGCUGGGA-3'; sgRNA2, 5'-CUUCCUCAGGGCUGGGAAGG-3'; and sgRNA3, 5'- UGUUCUCCUUGACGAUCUCG-3') and one control sgRNA (5'-GTACGTCGGTATAACTCCTC-3') were designed and cloned into the lentiviral vector plentiCRISPR v2. 293T cells (2.5×10^6) were transfected with the lentiviral vector expressing both the sgRNA and Cas9 (5 mg), the packaging plasmid (5 mg), and the VSV-G envelope expression plasmid (2.5mg) to generate lentiviral particles that were used to transduce A549 cells (2×10^5). After puromycin (2 μg/ml) selection, the transduced cells were single cell cloned. The knockout of NSUN2 expression in A549 and THP-1 cells was confirmed by Western blotting. Genome editing of the targeted region was also confirmed by PCR of exon 4 of NSUN2 from genomic DNA followed by sequencing.

Overexpression of SRP9 and SRP14 in NSUN2 and WT A549 cells. NUSUN2 knockout A549 cells or control sgRNA A549 cells (WT A549 cells) were transfected with 1 μg of empty vector (EV) or plasmid encoding SRP9 (pGFH-9) or SRP14 (pGFH-14c). After 48h, cells were infected with rVSV-GFP at an MOI of 0.1. At 18 hpi, GFP expression was captured by fluorescence microscopy, cell culture supernatants were harvested for determination of VSV titer by plaque assay, and total lysates were harvested for Western blot.

In vitro RNA transcription. DNA templates for the in vitro transcription of 7SL RNAs were generated by PCR with the primers listed in **Supplementary Table S 3**. 7SL RNA was synthesized using the T7 RNA polymerase in MEGAshortscript in vitro transcription kit (ThermoFisher, AM1354), followed by treatment of DNase, and were purified by phenol/chloroform extraction and ethanol precipitation. The final pellet was dried and eluted in RNase-free water.

Viral replication kinetics in A549 cells. For virus infection, confluent A549 cells were infected with rgRSV at an MOI of 0.1, rVSV-GFP at an MOI of 0.1, or hMPV at an MOI of 0.5. After incubation at 37°C for 1 h, the virus inoculum was removed and fresh DMEM with 2% FBS was added and the infected cells were incubated at 37 °C. At different time points post-infection, the cell culture supernatant and cells were harvested by three freeze-thaw cycles, followed by centrifugation at 3,000*g* at 4°C for 15 min. rgRSV, rVSV-GFP, and hMPV virus titer was measured by $TCID_{50}$ assay, plaque assay, and immunostaining plaque assay, respectively.

Real-time RT-PCR. RSV genome, antigenome, and mRNA were quantified by real-time RT-PCR. A549 cells were infected with rgRSV at an MOI of 0.1. At 18, 24, 36, and 48 post-infection, total RNA was isolated from cells using TRIzol (Life Technologies). Viral genome or antigenome copies were quantified by real-time RT-PCR using two primers specifically targeting the RSV leader sequence and GFP gene. Poly (A)-containing viral mRNAs were isolated from total RNA using oligo$(dT)_{23}$ (SigmaAldrich) according to the manufacturer's recommendations. The NS1, G, and N mRNA copies were quantified by real-time RT-PCR using two primers targeting the viral NS1, G, and N genes, respectively. The level of human β-actin mRNA was used to normalize each sample. For RPPH1 and 7SL RNAs, total RNA was isolated and purified from cells using TRIzol

reagent, and cDNA was synthesized using the Random primer. To determine shielded and unshielded 7SL RNAs, whole cells were treated with or without 0.1% Triton X-100, followed by incubation with or without micrococcal nuclease (MNase) at 37°C for 30 min. After MNase treatment, RNA was purified using TRIzol reagent. The qPCR primers for the assay are listed in the **Supplementary Table 3**.

RSV titration by $TCID_{50}$ assay. rgRSV titer was determined by $TCID_{50}$ assay in HEp-2 cells. Briefly, 10-fold serial dilutions of rgRSV were added to confluent HEp-2 cells in 96-well plates. The infected cells were incubated at 37°C for 5 days. Numbers of infected wells were counted, and $TCID_{50}$ values were calculated by Reed and Muench method. Same protocol was used for SeV-GFP.

VSV titration by plaque assay VSV titers were determined by plaque assay on Vero cells. Briefly, Vero cells were infected with 400 μl 10-fold serial dilutions of VSV for 1 h. And then overlaid with agarose gel. After 24 h, the cells were fixed with 10% neutral buffered formaldehyde at room temperature for 1 h and stained with crystal violet to count the plaques. Same protocol was used for PDCoV plaque assay.

hMPV titration by immunostaining plaque assay. Vero E6 cells were seeded in 24-well plates, infected with serial dilutions of hMPV, and overlaid with methylcellulose. At day 5 of infection, cells were fixed with 10% neutral buffered formaldehyde at room temperature for 30 min. Then the mixture of overlay and formaldehyde was removed. Cells were permeabilized in PBS containing 0.4% Triton X-100 at room temperature for 10 min and blocked at 37 °C for 1 h using

1% bovine serum albumin (BSA) in PBS. The cells were then incubated with anti-hMPV N protein primary monoclonal antibody (Millipore) at a dilution of 1:2,000 overnight at 4 °C, followed by incubation with horseradish peroxidase (HRP)-labelled goat anti-mouse secondary antibody (Thermo Scientific) at a dilution of 1:5,000. After incubation with 3-amino-9-ethylcarbazole chromogen substrate (Sigma), positive cells were visualized under a microscope. The viral titer was calculated as the number of plaque-forming units (PFU) per ml.

RSV and VSV replication in NSUN2-KO and control sgRNA-transduced A549 cells. Confluent NSUN2 knockout A549 cells or control sgRNA A549 cells were infected with rVSV- or rgRSV at an MOI of 0.1. At 12 and 24 h post-infection, GFP expression was captured by fluorescence microscopy, and cells were fixed by 10% neutral buffered formaldehyde and percent of GFP-positive cells was quantified by flow cytometry. Cell culture supernatants were harvested for determination of VSV and RSV titer by plaque assay and $TCID_{50}$ assay respectively. Total lysates were harvested for Western blot.

Western blot. A549 cells were infected with rgRSV, rVSV-GFP or hMPV at an MOI of 0.1 or 0.5. At indicated time points, cells were harvested and lysed in RIPA buffer (Abcam). Proteins were separated by 12% SDS-PAGE and transferred onto a Hybond ECL nitrocellulose membrane (Amersham, Piscataway, NJ) in a Trans-Blot Semi-Dry electrophoretic transfer cell (Bio-Rad, Hercules, CA). The blots were first blocked with phosphate-buffered saline supplemented with 0.02% Tween (PBST) containing 5% skim milk and then incubated with a primary antibody. After being washed with PBST three times (15 min per wash), the blot was incubated with a horseradish peroxidase (HRP)-conjugated secondary antibody. After being washed with PBST three times (15

min per wash), the blots were visualized with SuperSignal West Pico Chemiluminescent Substrate (Thermo Scientific, Pittsburg, PA) and exposed to Kodak BioMax MR film (Kodak, Rochester, NY). β-Actin was used as a loading control.

Fluorescence microscopy and flow cytometry. A549 cells were infected with rgRSV, rVSV-GFP, rSeV-GFP, or rHSV-GFP at an MOI of 0.1, and GFP expression was monitored at the indicated times by fluorescence microscopy. At the indicated time points, cells were trypsinized and fixed in 4% paraformaldehyde solution and the number of GFP-positive cells was quantified by flow cytometry using Attune NxT Flow Cytometer (ThermoFisher Scientific). The mock-infected cells (GFP negative) were used for gating controls. Then, the numbers of GFP-positive and GFP-negative cells in virus-infected cells were counted. Attune NxT software was used to collect and analyze the data. The percentage of GFP-positive cells was calculated.

Measurement of interferon in virus-infected or RNA-transfected cells. For virus infection, A549 cells were infected by hMPV, rgRSV, rSeV-GFP, or rVSV-GFP at MOI of 4.0 or 1.0, cell supernatants were harvested at the indicated time points after infection and IFN-β concentrations were determined by commercial enzyme-linked immunosorbent assays (ELISA) according to the manufacturer's instructions (Human IFN Beta ELISA Kit, PBL). Known concentrations of human IFN-β were used to generate the standard curve. For virion RNAs transfection, 2×10^7 copies of virion RNA of hMPV, rgRSV, or rVSV-GFP were transfected into A549 cells in 24-well plates. At 12 h and 16 h after transfection, culture medium was harvested for IFN-β quantification by ELISA.

For 7SL RNA transfection, 7SL RNAs were treated with or without Alkaline Calf Intestinal Phosphatase (CIP) (NEB, M0247S) at 37 °C for 10 min. After inactivation of CIP at 80 °C for 2 min, 7SL RNAs were further purified by TRIzol reagent. A549 cells in 24-well plates were transfected with CIP-treated or untreated RNA by Lipofectamine 3000. At 12 h and 24 h after transfection, culture medium was harvested for IFN-β quantification by ELISA.

Immunoprecipitation assay of RIG-I and RNA. HEK293T cells were transfected with pEF-BOS-RIG-I-Flag plasmid for 24h, cells were lysed in lysis buffer (Abcam, ab152163) and harvested after centrifugation at 13,000g for 10 min, and then the cell lysis were incubated with Anti-Flag M2 magnetic beads (Sigma-Aldrich, M8823) at room temperature for 80 min. The purified RIG-I protein were treated with or without RNase A and inoculated with or without in vitro-transcribed 7SL RNAs at room temperature for 60 min, beads with protein-RNA complex were washed in lysis buffer three times and total RNA was extracted from beads using TRIzol reagent and quantified by real-time RT-PCR.

RNA isolation. For virus-infected or uninfected wild-type, sgRNA transduced control, and NSUN2 knockout A549 cells, cellular total RNA was isolated with TRIzol reagent (Invitrogen) following manufacturer's protocol by isopropanol precipitation. When extracting rRNA-depleted total RNA for sequencing m^5C in RNA, RiboMinus™ Eukaryote System v2 (Invitrogen™) was further used for rRNA removal. When extracting $polyA^+$ RNA for sequencing m^5C in RNA, Dynabeads™ mRNA DIRECT™ Purification Kit (Invitrogen™) was used for $polyA^+$ RNA enrichment. When preparing total RNA for a typical RNA-seq, the total RNA was directly used for making libraries because of the rDNA removal steps within the protocol of SMARTer®

Stranded Total RNA-Seq Kit v2. Sample information for high-through sequencing was summarized in **Supplementary Table 4**.

Bisulfite sequencing for m^5C site detection. rgRSV-infected or VSV-infected NSUN2 knockout and sgRNA transduced control A549 cells, and HIV-1-infected NSUN2 knockout and sgRNA transduced control THP-1 cells were prepared as described (2 replicates each, one 10-cm plate per replicate). After extracting the rRNA-depleted total RNA, ~200 ng RNA was fragmented into 50-70 nt length using Na_2CO_3/$NaHCO_3$ buffer (pH 9.2) and heated at 95°C for 3 min, followed by purification with Oligo Clean & Concentrator (Zymo Research). ~50 ng was saved as "input" and the remainder was subjected to EZ RNA Methylation Kit (Zymo Research) for bisulfite treatment. 3'- and 5'-end repair was conducted for "input" and bisulfite-treated RNA by T4 Polynucleotide Kinase (EK0032, Thermo Fisher Scientific). RNA was mixed with 5 μL of 10× T4 Polynucleotide Kinase Reaction Buffer (B0201S, NEB) and 5 μL of T4 PNK, diluted to a final volume of 50 μL, and incubated at 37 °C for 1 h; then 2 μL of T4 PNK and 5 μL 10 mM ATP were added for another incubation 37 °C for 30 min, followed by Oligo Clean & Concentrator purification. To perform 3'-adaptor ligation, ~6 μL repaired RNA fragments were incubated with 1.0 μL 3'-Adaptor (5'App-NNNNN ATCACGAGATCGGAAGAGCACACGTCT-3SpC3) at 70 °C for 2 min and immediately placed on ice. 10 μL 3′ Ligation Reaction Buffer (2×) (NEB) and 3 μL 3′ Ligation Enzyme Mix (NEB) were added to the RNA-adapter mixture. The reaction was incubated at 25 °C for 2 h followed by 16 °C for 10 h. Then 1.0 μL SR RT Primer for Illumina (NEB) was added to the mixture, followed by 5 min at 75°C, 15 min at 37°C, 15 min at 25°C, and then on ice. The denatured 1.0 μL 5'-Adaptor (5'-GUUCAGAGUUCUACAGUCCGACGAUCNNNNN-3') was added into the mixture, together with 1.0 μL 5′ Ligation Reaction Buffer (10×) (NEB) and 2.5 μL

5′ Ligation Enzyme Mix (NEB). The reaction was incubated at 25 °C for 4 h, followed by RNA Clean & Concentrator purification

The purified RNA was mixed with 4 μL 5× SSIV Buffer (Thermo Scientific), 2 μL of 10 mM dNTP Solution Mix (NEB), 1 μL 100 mM DTT, 1 μL of RNaseOUT Recombinant Ribonuclease Inhibitor (Thermo Scientific), and 1 μL of SuperScript IV Reverse Transcriptase (Thermo Scientific). The reaction was diluted to 20 μL and incubated at 50°C for 30 min. 1.0 μL of RNase H (NEB, M0297L) was then added and the reaction was incubated at 37 °C for 20 min. The cDNAs were purified by Oligo Clean & Concentrator (Zymo Research). The libraries were amplified using the SR Primer for Illumina (NEB) and indexed primers (from NEBNext Multiplex Oligos for Illumina). All libraries were sequenced on Illumina NovaSeq 6000 with single-end 100 bp read length.

RNA-seq. NSUN2 knockout and control sgRNA-transduced A549 cells were prepared as described (3 replicates each, one 10-cm plate per replicate). Then ~50 ng purified cellular total RNA was subjected to library construction with SMARTer® Stranded Total RNA-Seq Kit v2. All libraries were sequenced on Illumina NovaSeq 6000 with paired-end 50 bp read length.

Cellular dsRNA isolation and dsRNA-seq. NSUN2 knockout and control sgRNA-transduced A549 cells were prepared as described (3 replicates each, four 15-cm plates per replicate). For each sample, 250 μL of Protein G Dynabeads (Invitrogen™, 10004D) was washed twice and resuspended in 1 mL of IP wash buffer (50 mM HEPES, pH 7.5, 150 mM NaCl, 1 mM $MgCl_2$, 0.5% NP-40). 25 μg of anti-dsRNA mAb (J2) was added to the beads and incubated for 1 hour at room temperature, followed by another 1-2 hours at 4 °C. Cultured cells were washed once with

cold DPBS. Each plate of cells was soaked in 5 mL cold DPBS and collected by cell lifters, combining 5 plates for each sample. The cell suspension was spun at 300 g at 4 °C for 2 min. Cells were resuspended in 1 mL NP-40 lysis buffer (10mL solution: 50 mM HEPES pH 7.5, 150 mM NaCl, 2 mM EDTA, 10 mM $MgCl_2$, 0.5% NP-40, plus 50 µL TURBO™ DNase (2 U/µL, AM2238, Invitrogen), 500 µL SUPERase•In™ RNase Inhibitor (20 U/µL, AM2694, Invitrogen), Pierce™ EDTA-free Protease Inhibitor Tablet) and incubated at 4 °C for 30 min. The lysate was spun at 16,000 g at 4 °C for 5 min. The supernatant was transferred to a new Eppendorf tube and 10 µL of that was kept as the "input". The lysate was diluted to 4.75 mL with IP wash buffer. 250 µL of J2-Dynabeads was added to the lysate and incubated at 4 °C for 2 hours. The magnetic beads were washed once with 1 mL IP wash buffer and transferred to a new Eppendorf tube. The beads were further washed twice by 1 mL of IP wash buffer. Input RNA and J2-bound dsRNA were extracted using TRIzol, with small RNA (< 200 nt) removal by RNA Clean & Concentrator (Zymo Research). The purified dsRNA was subjected to library construction with SMARTer® Stranded Total RNA-Seq Kit v2. All libraries were sequenced on Illumina NovaSeq 6000 with paired-end 50 bp read length.

Identification of bisulfite induced misincorporation. The sequencing data was all trimmed with cutadapt tool to remove adapters and low-quality reads. PCR duplicates were removed with BBMap tool (https://sourceforge.net/projects/bbmap/), 5-mer random barcodes at reads ends were trimmed, and low-quality or short reads (less than 30 nt) were removed using cutadapt tool. Remaining reads were aligned to the converted human genome (hg38, C->T or G->A converted, by Bismark-0.22.3 tool, https://github.com/FelixKrueger/Bismark/releases) using Tophat2 (version 2.1.1) and bowtie2 (version 2.3.5.1) allowing at most three mismatches. The

generated .bam files were split into positive and negative strands and sorted using Samtools (http://samtools.sourceforge.net/). Sequence variants were identified by measuring the base composition at each position using fine-tuned bam-readcount (https://github.com/genome/bam-readcount). The generated bam-readcount results were parsed and analyzed by in-house scripts. All cytidine sites in RNA were converted into uridine after bisulfite treatment, and the sites showing T→C mutations are the m^5C candidate sites. T to C mutation ratio at each m^5C candidate site were calculated by data output from bam-readcount pipeline and confirmed by direct visualization through IGV software (https://software.broadinstitute.org/software/igv/). In summary, an m^5C candidate site needs to satisfy the criterion in its misincorporation profile: (1) the T→C mutation count of this candidate site should be above 5; (2) the mutation ratio (C→A or G or T) of this candidate site needs to be zero in "input" library; (3) the T→C mutation ratio of this candidate site in "bisulfite treated" library is at least 20% and the candidate site does not appear within a cluster of multiple successive T→C mutations. (4) all T→C misincorporation signatures must appear at the internal positions within reads, instead of occurring at reads ends. All confident sites with T→C mutation above 20% were used for downstream study, like investigating NSUN2-hypomethylated sites. We focused on the m^5C sites that displayed a significant reduction (≥ 10%) of methylation fraction after NSUN2 depletion.

Differential expression analysis of cellular host RNA. The input of bisulfite sequencing library (for RNA m^5C detection) is equivalent to regular RNA-seq, therefore we quantified the gene-level read counts of input samples that aligned to hg38 for differential gene expression analysis. Cufflinks and Cuffdiff were used to make inferential tests where differentially expressed genes

were identified at FDR < 0.05 cut-off. Gene ontology analysis was performed using the online analysis software DAVID v6.8 (https://david.ncifcrf.gov) and REViGO tool (http://revigo.irb.hr).

Transcription assay for non-coding RNA (ncRNA). Confluent NSUN2 KO A549 cells and control sgRNA transduced A549 cells were metabolically labeled with 0.5 mM of 5-ethynyl uridine (EU). For side-by-side comparison, A549 cells were transfected with siNSUN2 or control siRNA, which were also metabolically labeled with 0.5 mM of EU at 48 h post-transfection.

In both cases, A549 cells in 10-cm plates were prepared. A 5-ml volume of culture medium with 0.5 mM EU was added to each plate and incubated at 37 °C for 10, 20, 30, and 90 min after adding EU. Cells were washed once with cold DPBS and total RNA was immediately extracted with TRIzol and isopropanol precipitation, followed by adding the biotin-tagged ssDNA spike-in probe (4). Cellular nascent RNA was enriched by biotin pulldown based on the standard protocol of the Click-iT Nascent RNA Capture Kit (Invitrogen, C10365). All RNA samples were denatured at 80 °C for 2 min before conducting RT with SuperScript™ II Reverse Transcriptase (Invitrogen™, 18064022). The levels of RPPH1, 7SL RNA, and 7SK RNAs were quantified by RT-qPCR. All RNA levels were normalized to the RNA levels at 10-min time point in wild-type A549 cells. Biotin-tagged ssDNA spike-in probe was used as the internal standard for normalization of each time point.

Stability assay for non-coding RNA (ncRNA). Confluent NSUN2 KO A549 cells and control sgRNA transduced A549 cells were treated with Pol III transcription inhibitor ML-60218 at a final concentration of 30 μM. At 0, 3, and 6h after adding ML-60218. Cells were washed once with cold DPBS, and total RNA was immediately extracted with TRIzol and isopropanol precipitation.

DNase I (NEB, M0303L) treatment was conducted to remove any DNA contamination. Approxiamtely 300 ng RNA per sample was subjected to reverse transcription with PrimeScript™ RT reagent Kit (Perfect Real Time) (Takara Bio, RR037A). The levels of RPPH1, 7SL RNA and 7SK RNAs were quantified by RT-qPCR. RNA levels were normalized to the RNA level at 0-hour time point in wild-type and NSUN2 KO cells, respectively. Human 18S rRNA level was used as the internal standard for normalization of each time point.

Generation of NSUN2-knockdown HBE culture. Primary, well-differentiated human bronchial epithelial (HBE) cultures were grown on collagen coated Transwell inserts (Corning Inc., Corning, NY), as previously described (5-7). Briefly, progenitor cells were isolated from bronchial tissues from a healthy human donor (under IRB protocol no. 009-02). Progenitor cells were seeded on collagen-coated Transwells and 24 h later, transduced by a puromycin- selectable lentivirus expressing sgRNA targeting NSUN2 or control sgRNA. After 4 h incubation on a rocking platform in a 37ºC, 5% CO2 incubator, the inoculums were removed and 100 µl of apical medium containing puromycin (2µg/ml) was added to select the cells which had received the lentivirus. Upon reaching confluency and forming tight junctions, the apical medium was removed, and the basal medium was replaced with Pneumacult-ALI (Stem Cell Technologies Inc., Vancouver, BC, Canada) every 2 to 3 days for 3 weeks to stimulate differentiation at the air-liquid interface. At week 4, one well of HBE transduced by NSUN2 sgRNA and another well of control sgRNA was lysed by RIPA buffer (Abcam) for Western blot analysis using antibody against NSUN2 or β-actin.

Replication, spread, and cytokine production in HBE cultures. After confirming the knockdown or knockout of the NSUN2 gene in HBE cultures, the apical surface of well-

differentiated HBE cells in Transwells was washed 5 times with 100 µl DMEM and the basal medium was changed. GFP-expressing rgRSV virus, 400 pfu in 100 µl DMEM was added to the apical surface of NSUN2-knockdown HBE or control sgRNA-treated HBE culture. At days 1, 2, and 3 post-infection, fluorescent cells were visualized and photographed with an EVOS2 fl inverted fluorescence microscope (Life Technologies). The amount of the HBE culture expressing GFP-positive cells was quantified from a digital image using the Image J Software. In addition, released virus was collected by adding 100 µl of DMEM to the apical surface of HBE cultures, gently rocking for 30 min, and collected to quantify and apically released virus, cytokines and chemokines. The 0.5 ml of medium on the basal side of the filter was collected. Virus yield in the apical wash was determined by titration on HEp2 cells. Major cytokines and chemokines released from the apical and basolateral surfaces were quantified by a flow cytometer bead assay (LEGENDplex; Biolegend, San Diego, CA).

RSV infection in NSUN2-knockout and wild type mice. Ten 4-6-week-old female wild type ($NSUN2^{+/+}$) mice were divided into two groups (n=5): the first group was intranasally inoculated with 4×10^5 $TCID_{50}$ of rgRSV in 30 µl PBS, and the second group was intranasally inoculated with 30 µl PBS and served as mock-infected controls. Similarly, ten 4-6-week-old female $NSUN2^{+/-}$ mice were divided into two groups (n=5): the first group was intranasally inoculated with 4×10^5 $TCID_{50}$ of rgRSV in 30 µl PBS, and the second group was intranasally inoculated with 30 µl PBS and served as mock-infected controls. At day 3 post-inoculation, all mice were euthanized, and the nasal turbinate and the right lung from each mouse were removed, weighed, and homogenized in 500µL of PBS. Total RNA was extracted for

quantification of RSV RNA and type I IFN (IFNα and IFNβ) mRNA. The left lung was fixed in 4% neutral buffered formaldehyde for histology.

VSV infection in NSUN2-knockout and wild type mice. Ten 4-6-week-old female wild type ($NSUN2^{+/+}$) mice were divided into two groups (*n*=5): the first group was intranasally inoculated with 10^6 PFU of VSV in 30 µl PBS, and the second group was intranasally inoculated with 30 µl PBS and served as mock-infected controls. Similarly, ten 4-6-week-old female $NSUN2^{+/-}$ mice were divided into two groups (*n*=5): the first group was intranasally inoculated with 10^6 PFU of VSV in 30 µl PBS, and the second group was intranasally inoculated with 30 µl PBS and served as mock-infected controls. At day 3 post-inoculation, all mice were euthanized, and the right lung and brain from each mouse were removed, weighed, and homogenized in 500µL of PBS. VSV titers in lungs and brain were quantified by plaque assay. Total RNA was extracted from lung tissues for quantification of type I IFN (IFNα and IFNβ) mRNA. The left lung and brain was fixed in 4% neutral buffered formaldehyde for histology.

Design of vivo-MO. Two pairs of NSUN2 vivo-phosphorodiamidate morpholino oligomers (vivo-MO) and one control vivo-MO were synthesized by Gene Tool LLC (Corvallis, OR). One NSUN2 MO targets at 5'UTR of NSUN2 to block ribosome assembly, and the sequence is 5' CTGCACACGCGGAGCGCACACAG 3'. The second NSUN2 MO targets exon 4 (106 bases) causing a frameshift of the downstream sequence. The sequence for the second NSUN2 MO is 5' CGCTCACAGAACCCACTTACAGACT 3'. The sequence of the non-targeting control vivo-MO is 5' CCTCTTACCTCAGTTACAATTTATA 3'. The vivo-morpholino oligomers were dissolved

in PBS at a concentration of 0.5 mM. To achieve maximum knockdown efficiency, equal amounts of the two NSUN2 vivo-MO were mixed and used for in vivo delivery.

RSV infection in NSUN2 intranasally knockdown mice. Fifteen 6-week-old specific pathogen free (SPF) female C57BL/6J mice were randomly divided into 3 groups (*n*=5). Mice in groups 1 and 2 were intranasally inoculated with NSUN2-specific vivo-MO or control vivo-MO (12 mg/kg), respectively, for three consecutive days. Mice in group 3 were inoculated with PBS and served as normal controls. At day 4, mice in groups 1 and 2 were intranasally inoculated with 20 μl of PBS containing 2×10^5 $TCID_{50}$ of rgRSV. At day 3 post-inoculation, all mice were euthanized, and the nasal turbinate and the right lung from each mouse were removed, weighed, and homogenized in 500μL of PBS. Total RNA was extracted for quantification of RSV RNA, NSUN2 mRNA and type I IFN mRNA. The left lung was fixed in 4% neutral buffered formaldehyde for histology.

VSV infection in NSUN2 intravenously knockdown mice. Fifteen 6-week-old female C57BL/6J mice were randomly divided into 3 groups (*n*=5). Mice in groups 1 and 2 were intravenously injected with NSUN2-specific vivo-MO and control vivo-MO (12 mg/kg per mouse), respectively, for three consecutive days. Mice in group 3 were intravenously injected with PBS and served as normal controls. At day 4, mice in groups 1 and 2 were intranasally inoculated with 20 μl of PBS containing 1.0×10^4 PFU of VSV Indiana strain. At day 3 post-inoculation, mice were terminated, half of the brain and the right lung from each mouse were collected, weighed, and homogenized in 500μL of PBS. Total RNA was extracted for quantification of VSV RNA, NSUN2 mRNA, and type I IFN mRNA. In addition, the VSV titer in the brain was determined by plaque assay. The left lung and half of brain were fixed in 4% neutral buffered formaldehyde for histology.

Determination of VSV titer in mouse brain. The brain from each mouse was weighed, and homogenized in 0.5 ml of DMEM. The brain was homogenized using a Precellys 24 tissue homogenizer (Bertin instruments, Rockville, MD) by following the manufacturer's recommendations. VSV titer in brain was determined by plaque assay.

Quantification of VSV and RSV RNA, NSUN2 mRNA, and IFN mRNA of mice tissue by real-time RT-PCR. Lung tissue was homogenized using a Precellys 24 tissue homogenizer (Bertin instruments). The mucosa from the nasal turbinates was homogenized by hand with a 0.90mm CoorsTek mortar and pestle (Golden, CO) and sterile sand. Total RNA was extracted from 150μL out of 500μL tissue and dissolved in 50μL RNase-free water. To measure RSV and VSV replication, genome RNA in the lungs and nasal turbinate was quantified by real-time RT-PCR using one primer annealing to the leader sequence and N gene complement sequence. In addition, reverse transcription (RT) was carried out using 2μL of total RNA and Oligo (dT)23 in 20μL system, and the synthesized cDNA was diluted 1:2 and used for real-time PCR to quantify NSUN2 mRNA (to measure knockdown of NSUN2) and type I IFN mRNA (IFN-α and IFN-β) (to measure the innate immune response). Primers used for qPCR are listed in **Supplementary Table 3.**

Lung and brain histology. After euthanizing the mice, the left lung of each animal was removed, inflated, and fixed with 4% neutral buffered formaldehyde. Fixed tissues were embedded in paraffin and cut by a microtome to generate 5 μm sections. Slides were then stained with hematoxylin-eosin (H&E) for the examination of histological changes by light microscopy.

Histopathological changes of the lungs were evaluated based on the extent of peribronchiolitis, perivasculitis, bronchiolitis, alveolitis, and interstitial pneumonia using a modification of the adapted criteria (8). Histopathological changes in the brain were evaluated based on the severity of encephalitis including neuronal necrosis, gliosis, neuronal satellitosis, mononuclear cell infiltration, and neuronophagia with lymphocytic perivascular cuffing(9).

Statistical analysis. Quantitative analysis was performed by either densitometric scanning of on X-ray film images or by using a phosphorimager (Typhoon; GE Healthcare) to capture the image and ImageQuant TL software (GE Healthcare) or ImageJ (NIH) for quantification. Statistical analysis was performed by one-way multiple comparisons using SPSS (v.8.0) statistical analysis software (SPSS) or student's *t* test. A P of <0.05 was considered statistically significant.

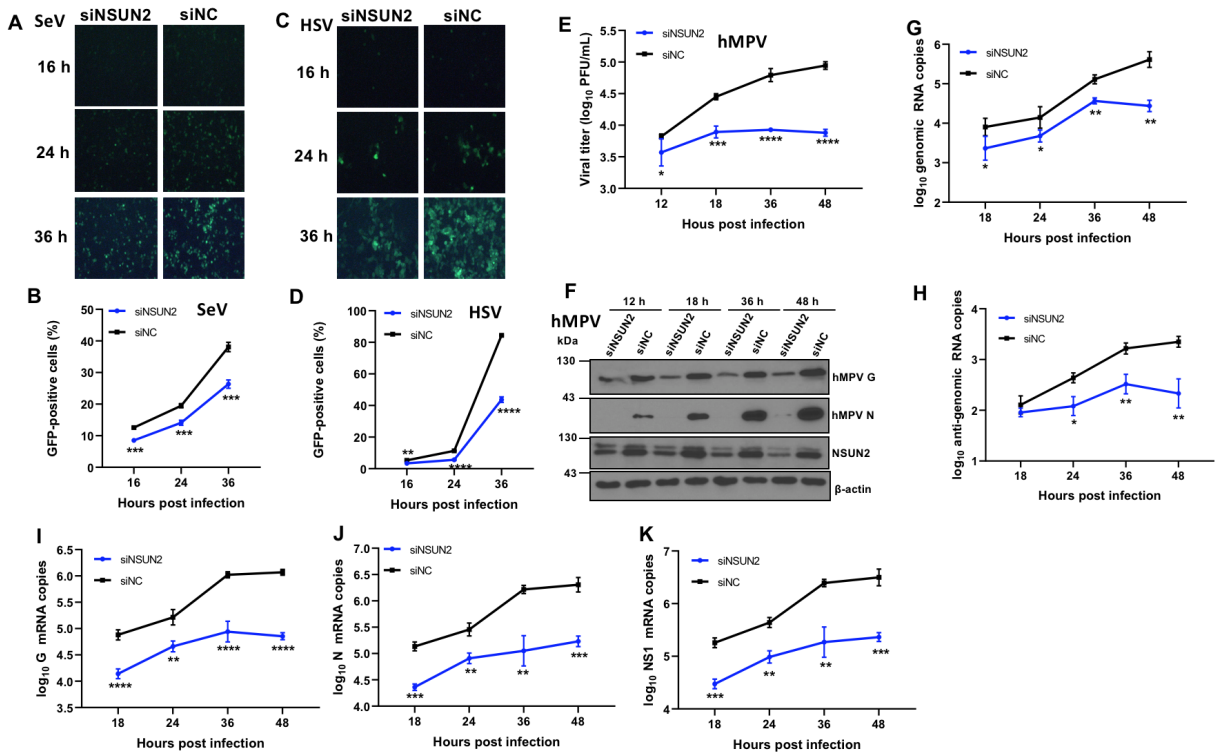

Fig.S1. NSUN2 depletion suppresses virus replication and gene expression. (**A-B). NSUN2 depletion suppresses SeV replication.** A549 cells were transfected with siNSUN2 or siNC, and were infected with rSeV-GFP at an MOI of 0.1. GFP images were monitored by fluorescence microscopy (A) and percent of GFP-positive cells quantified by flow cytometry (B). **(C-D). NSUN2 depletion suppresses HSV replication.** A549 cells were transfected with siNSUN2 or siNC, and were infected with rHSV-GFP at an MOI of 0.1. GFP images were monitored by fluorescence microscopy (C) and percent of GFP-positive cells quantified by flow cytometry (D). (**E-F). NSUN2 depletion suppresses hMPV replication.** A549 cells were transfected with siNSUN2 or siNC, infected with rhMPV at an MOI of 0.5, and hMPV titer in cell culture supernatants (E) and hMPV protein expression (F) and were determined. **(G-K) NSUN2 depletion reduces RSV genome replication and mRNA transcription.** A549 cells transfected with siNSUN2 or siNC, followed by infection with rgRSV at an MOI of 0.1, total RNA was isolated from the cells using TRIzol reagent. RSV genome (G), antigenome (H), G mRNA (I), N mRNA (J), and NS1 mRNA (K) were measured by real-time RT-PCR. RNA copies are the geometric mean titer (GMT) of three independent experiments ± standard deviation. Data were analyzed using Student's *t*-test and statistical differences were indicated as $*P < 0.05$; $**P < 0.01$; $***P < 0.001$; and $****P < 0.0001$.

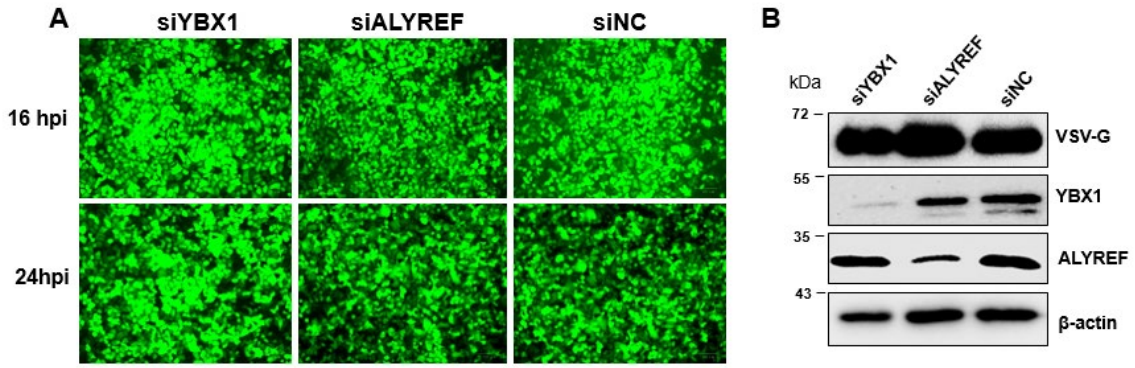

Fig.S2. Depletion of m^{5}C reader proteins does not significantly inhibit VSV replication. A549 cells were transfected with siYBX1, siALYREF, or siNC, respectively. At 48 h post-transfection, cells were infected with rVSV-GFP at an MOI of 0.1. At indicated times, GFP images were captured by fluorescence microscopy (**A**). Cell lysates harvested at 24 hpi were subjected to Western blot analyses using antibody specific to YBX1, ALYREF, and VSV G protein (**B**).

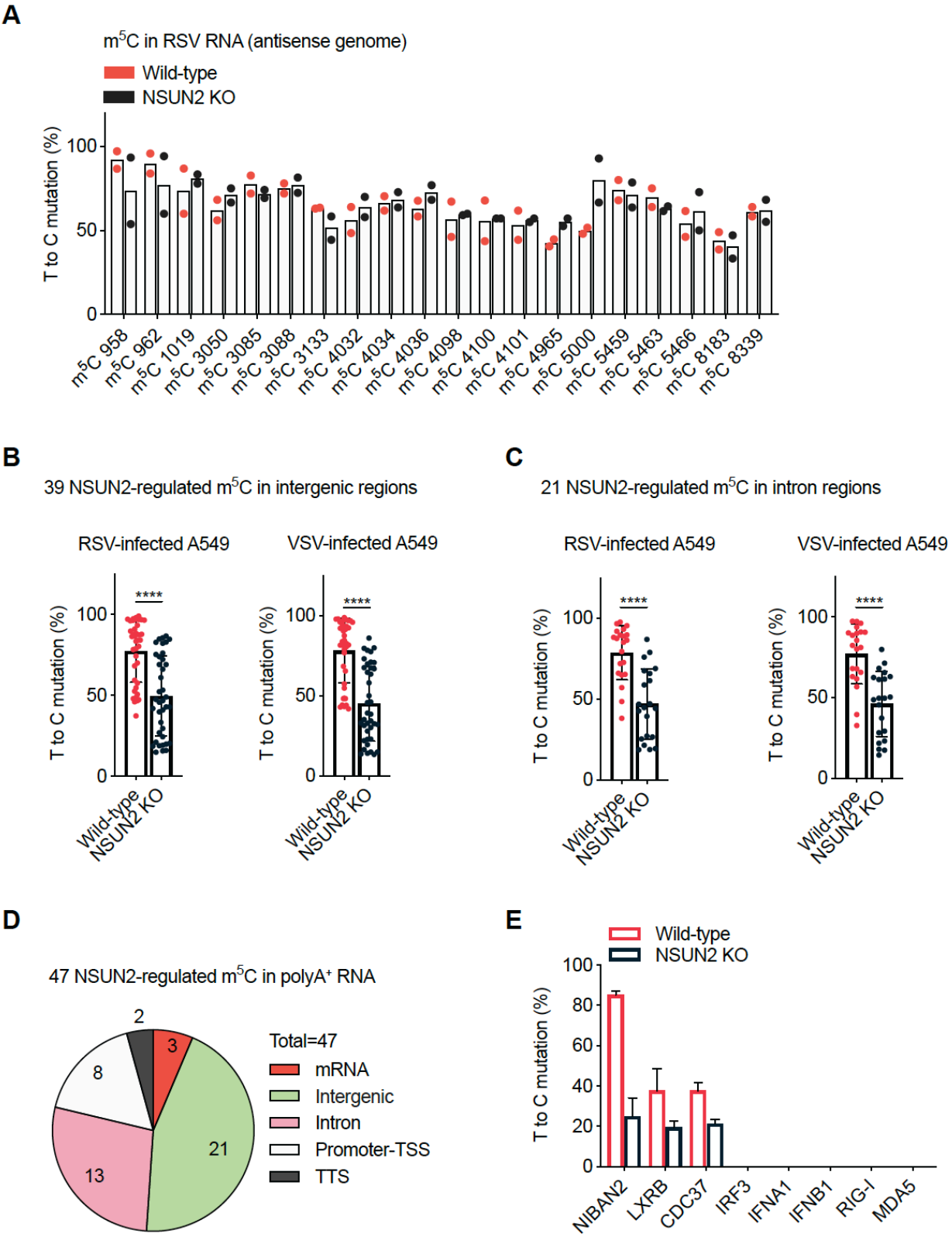
A
m5C in RSV RNA (antisense genome)
Wild-type
NSUN2 KO
T to C mutation (%)
100
50
0
m5C 958
m5C 962
m5C 1019
m5C 3050
m5C 3085
m5C 3088
m5C 3133
m5C 4032
m5C 4034
m5C 4036
m5C 4098
m5C 4100
m5C 4101
m5C 4965
m5C 5000
m5C 5459
m5C 5463
m5C 5466
m5C 8183
m5C 8339
B
39 NSUN2-regulated m5C in intergenic regions
RSV-infected A549
VSV-infected A549
****
T to C mutation (%)
Wild-type
NSUN2 KO
C
21 NSUN2-regulated m5C in intron regions
RSV-infected A549
VSV-infected A549
D
47 NSUN2-regulated m5C in polyA+ RNA
2
3
8
21
13
Total=47
mRNA
Intergenic
Intron
Promoter-TSS
TTS
E
Wild-type
NSUN2 KO
T to C mutation (%)
100
80
60
40
20
0
NIBAN2
LXRB
CDC37
IRF3
IFNA1
IFNB1
RIG-I
MDA5

Fig. S3. NSUN2 depletion regulates m^5C methylation in some host RNAs of A549 cells but not in virus-related RNA.

A, the mutation levels of 20 m^5C site in RSV viral RNA (genome) from NSUN2-knokout A549 cells *vs*. wild-type cells. **B**, the mutation levels of 39 NSUN2-regulated m^5C site in intergenic regions from NSUN2-knokout A549 cells *vs*. wild-type cells. **C**, the mutation levels of 21 NSUN2-regulated m^5C site in intron regions from NSUN2-knokout A549 cells *vs*. wild-type cells. For **B-C**, *P* values were determined using two-tailed t test for paired samples. ****$P < 0.0001$. **D**, the distribution of NSUN2-regulated m^5C sites in several major RNA species from A549 $polyA^+$ RNA. **E,** the mutation levels of three NSUN2-regulated m^5C site in mRNA from NSUN2-knokout A549 cells *vs*. wild-type cells. No m^5C sites were detected in other mRNAs such as IRF3, IFNA1, IFNB1, RIG-I, and MDA5.

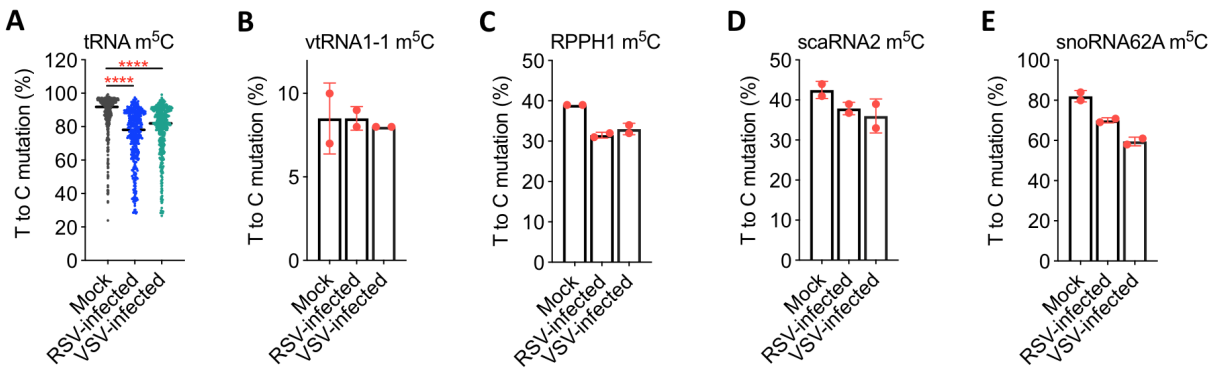

Fig. S4. Virus infection alters host m^{5}C methylome. Confluent A549 cells were infected with rgRSV or rVSV-GFP at an MOI of 0.1. Mock-infected A549 cells were used as controls. At 48h post-infection, total RNA was extracted from mock or virus-infected cells. After depletion of rRNA, the RNA was subjected to the bisulfite sequencing. **A**, the mutation levels of m^{5}C sites in cytoplasmic tRNAs from wild-type A549 cells (without viral infection) *vs*. RSV- or VSV-infected cells. *P* values were determined using Wilcoxon matched-pairs signed rank test for paired samples. ****$p < 0.0001$. **B**, the mutation levels of one m^{5}C site in RPPH1 RNA from wild-type A549 cells (without viral infection) *vs*. RSV- or VSV-infected cells. **C**, the mutation levels of one m^{5}C site in vault RNA (vtRNA1-1) from wild-type A549 cells (without viral infection) *vs*. RSV- or VSV-infected cells. **D**, the mutation levels of 2 m^{5}C sites in snoRNA 62A and 62B from wild-type A549 cells (without viral infection) *vs*. RSV- or VSV-infected cells. **E**, the mutation levels of one m^{5}C site in scaRNA2 from wild-type A549 cells (without viral infection) *vs*. RSV- or VSV-infected cells. For **B**-**E**, Mean values ± SD are shown; $n = 2$.

A: NSUN2-KO upregulated genes (vs. WT), in VSV-infected A549 cells.

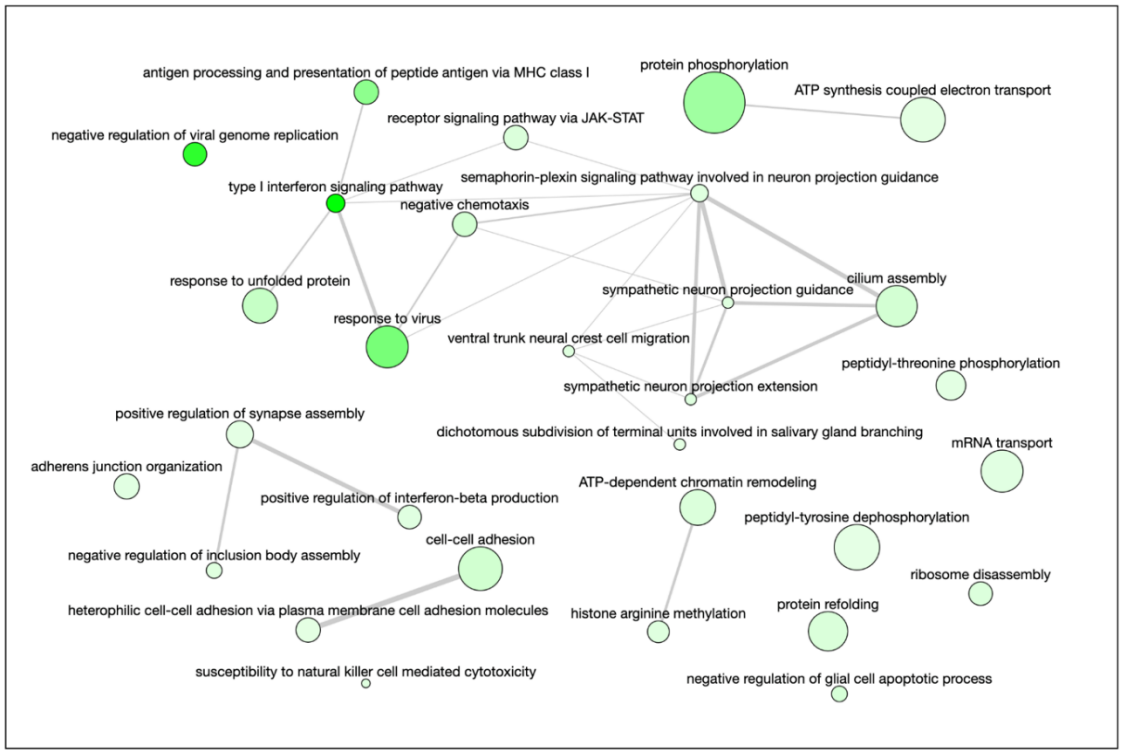

B. NSUN2-KO downregulated genes (vs. WT), in VSV-infected A549 cells.

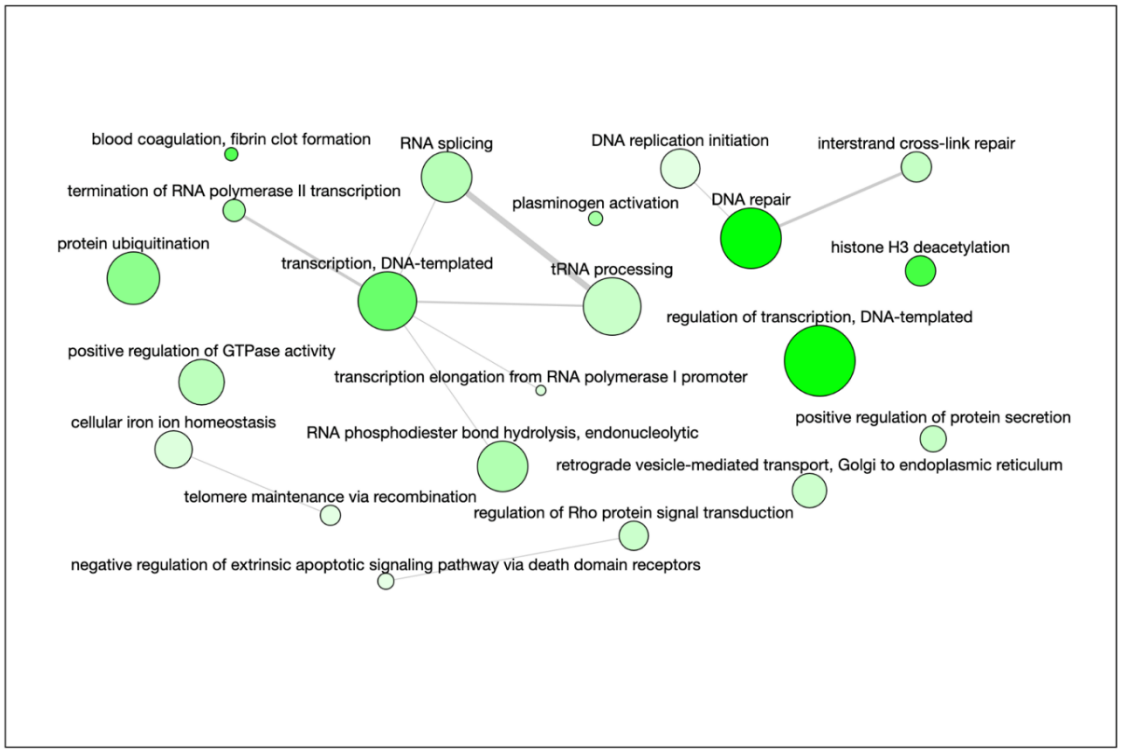

Fig. S5. NSUN2 depletion leads to an enhanced upregulation of type-I interferon signaling and antivirus immune response, and an elevated downregulation of DNA transcription and DNA repair. A, the correlation graph among enriched GO clusters of upregulated genes in VSV-infected NSUN2-knockout A549 cells (*vs*. VSV-infected wild-type A549 cells). **B**, the correlation graph among enriched GO clusters of downregulated genes in VSV-infected NSUN2-knockout A549 cells (*vs*. VSV-infected wild-type A549 cells).

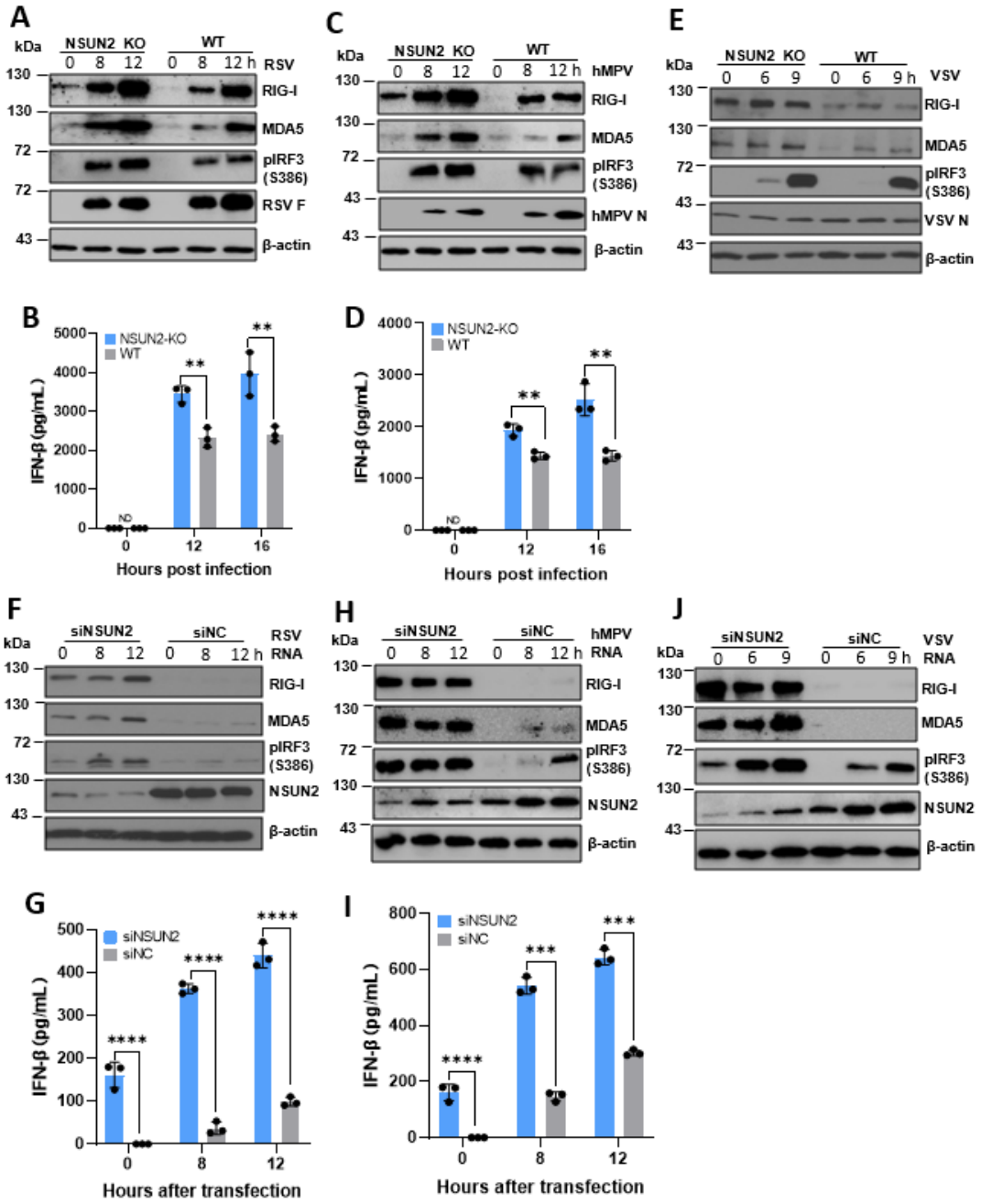

Fig. S6. NSUN2 depletion leads to the activation of a higher type I IFN signaling pathway. (A-D) NSUN2 knockout A549 cells induces a higher type I IFN after virus infection. NSUN2 knockout and control sgRNA transduced A549 cells were infected with rgRSV (A and B), hMPV (C and D), or rVSV-GFP (E) at an MOI of 4.0, 5.0, and 1.0, respectively. At indicated times, cell

lysates were subjected to Western blot (A, C, and E) using antibody against RIG-I, MDA5, phosphorylated IRF3 (pIRF3), and β-actin. IFN-β (B and D) in cell culture supernatants was measured by ELISA. **(F-I) NSUN2 knockdown induces a higher type I IFN after viral RNA transfection.** A549 cells were transfected with siRNA against NSUN2 or control siRNA, followed by transfection with virion RNAs (2×10^6 copies/well) of rgRSV (F and G), hMPV (H and I), or rVSV-GFP (J). At indicated time points, cell lysates were subjected to Western blot (F, H, and J) against RIG-I, MDA5, pIRF3, and β-actin. IFN-β (G and I) in cell culture supernatants was measured by ELISA. All data are from three (n= 3) independent experiments. Data were analyzed using Student's t-test and statistical differences were indicated as $^*P < 0.05$; $^{**}P < 0.01$; $^{***}P < 0.001$; and $^{****}P < 0.0001$.

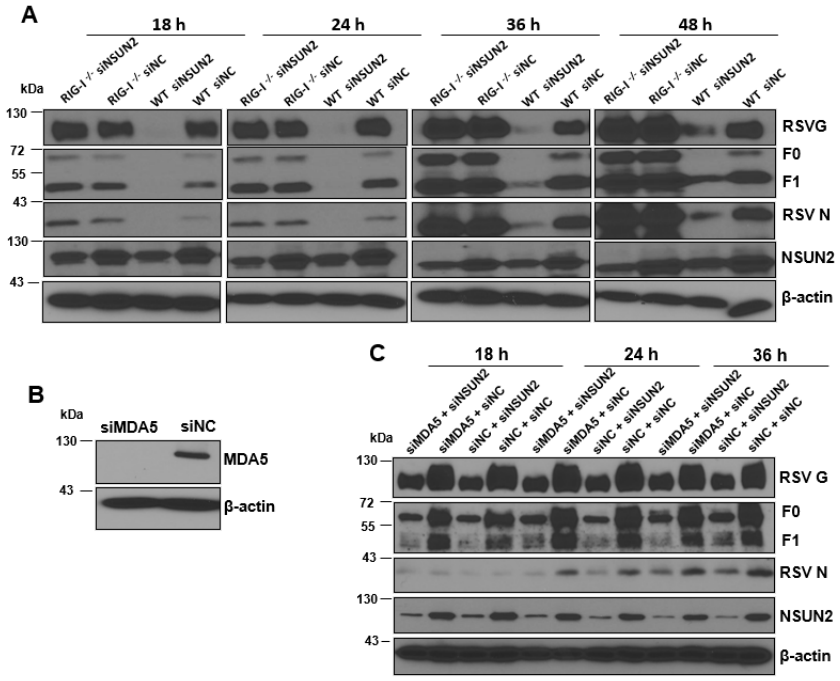

Fig.S7. m^{5}C deficiency-mediated antiviral response is dependent on RIG-I but not MDA5. (A) Confluent WT A549 cells and RIG-I-knockout (RIG-I $^{-/-}$) A549 cells were transfected with siRNA against NSUN2 or control siRNA, followed by infection with rgRSV at an MOI of 0.1. At the indicated time points, cell lysates were harvested for Western blot. (B) Western blot showing MDA5 efficiently knocked down by siRNA. (C) A549 cells were transfected with siRNA against NSUN2, MDA5, or both, followed by infection with rgRSV at an MOI of 1.0. At the indicated time points, cell lysates were harvested for Western blot (C).

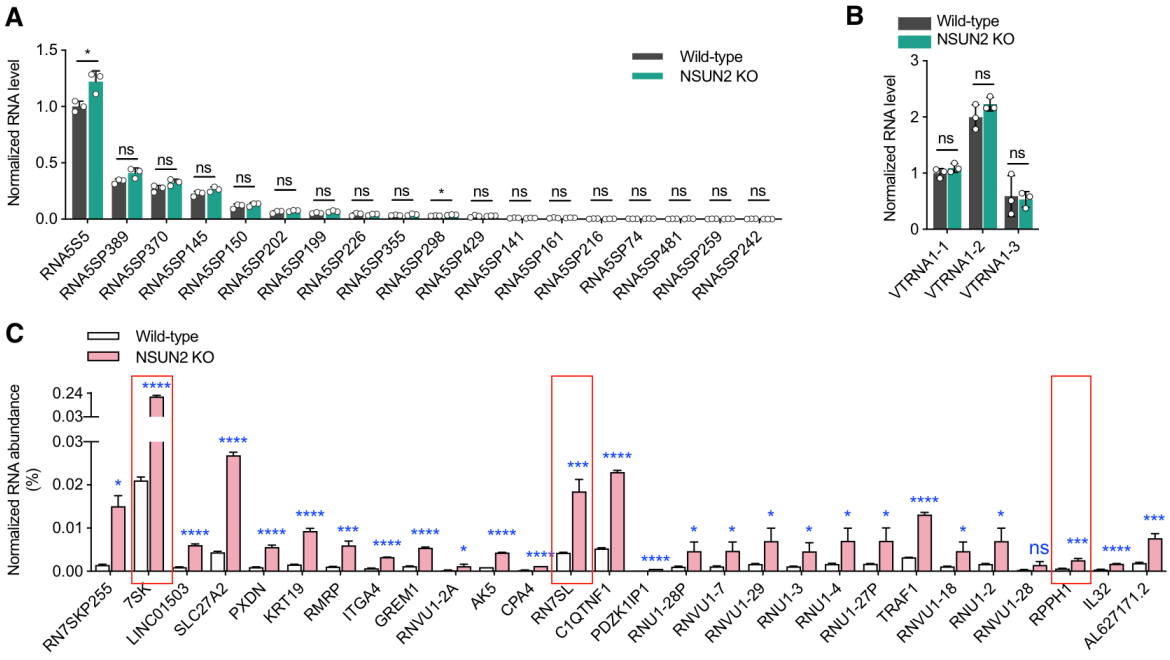

Fig. S8. NSUN2-depletion does not directly affect RNA level of 5S rRNA pseudogene and vault RNAs, but enhances the dsRNA feature of 7SL and 7SK RNAs.

A, the relative RNA levels of 5S rRNAs and its highly expressed pseudogenes in NSUN2-knockout A549 cells *vs*. the wild-type when without viral infection, which are transcribed by Pol III. **B**, the relative RNA levels of vault RNAs in NSUN2-knockout A549 cells *vs*. the wild-type when without viral infection, which are transcribed by Pol III. **C**, In dsRNA-seq, the relative RNA abundance of 28 genes with an increased level (above 3 folds) after NSUN2 depletion (*vs*. wild-type). Y axis: the percentage showing how much the reads count from one specific gene occupies in all dsRNA antibody IP-enriched genes. For **A**-**C**, mean values ± SD are shown; n = 3 biologically independent samples. *P* values were determined using unpaired *t*-test. **P* < 0.05; ***P* < 0.01; ****P* < 0.001; *****P* < 0.0001.

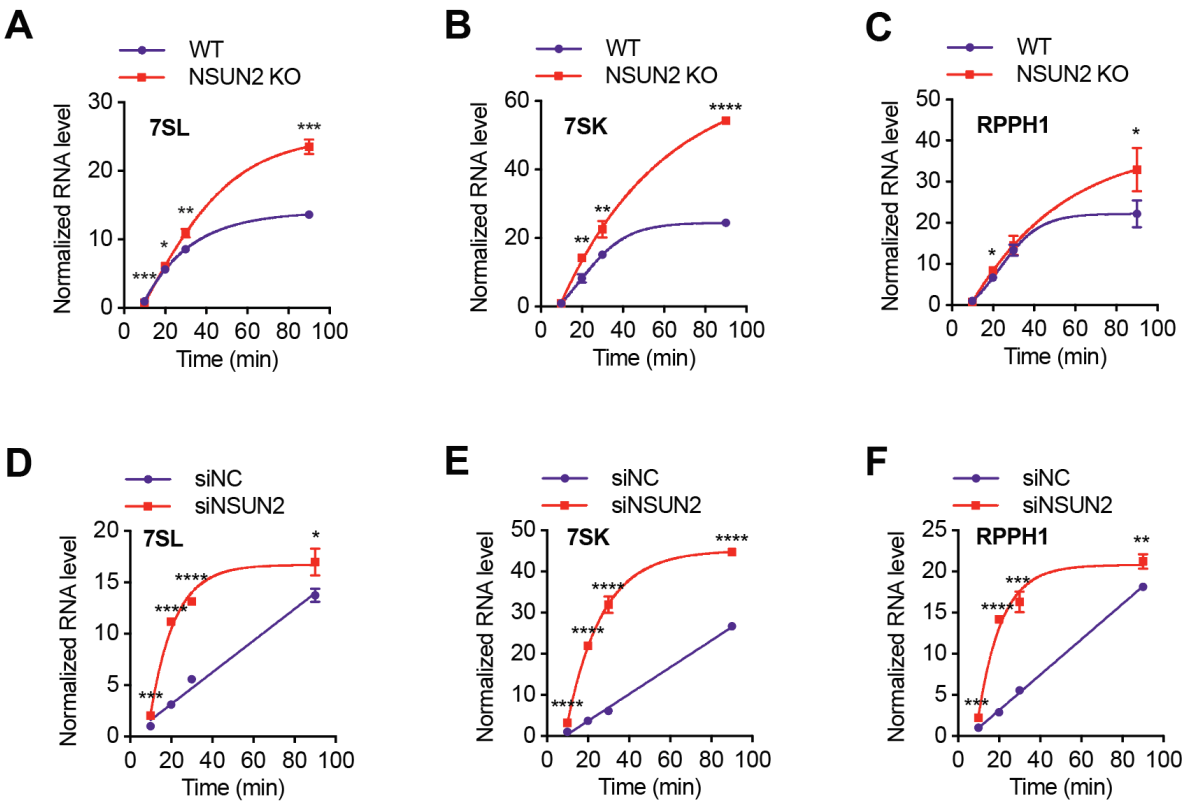

Fig.S9. NSUN2 depletion enhances transcription of ncRNAs. **A**, The transcription rate for 7SL RNA in NSUN2 KO A549 cells *vs*. WT A549 cells. **B**, The transcription rate for 7SK RNA in NSUN2 KO A549 cells *vs*. WT A549 cells. **C**, The transcription rate for RPPH1 RNA in NSUN2 KO A549 cells *vs*. WT A549 cells. For **A**-**C**, RT-qPCR quantification was conducted on isolated EU-labeled RNA at time points of 10, 20, 30, and 90-min, respectively. All RNA levels were normalized to 10-min time point in WT A549 cells. **D**, The transcription rate for 7SL RNA in siNSUN2-treated A549 cells *vs*. control siRNA-treated cells. **E**, The transcription rate for 7SK RNA in siNSUN2-treated A549 cells *vs*. control siRNA-treated cells. **F**, The transcription rate for RPPH1 RNA in siNSUN2-treated A549 cells *vs*. control siRNA-treated cells. For **D**-**F**, RT-qPCR quantification was conducted on isolated EU-labeled RNA at time points of 10, 20, 30, and 90-min, respectively. All RNA levels were normalized to 10-min time point in control siRNA-treated cells. For **A**-**F**, Mean values ± SD are shown; $n = 3$. Biotin-tagged ssDNA spike-in probe was used as the internal standard for normalization of each time point. *P* values were determined using unpaired t-test. *$P < 0.05$; **$P < 0.01$; ***$P < 0.001$; ****$P < 0.0001$.

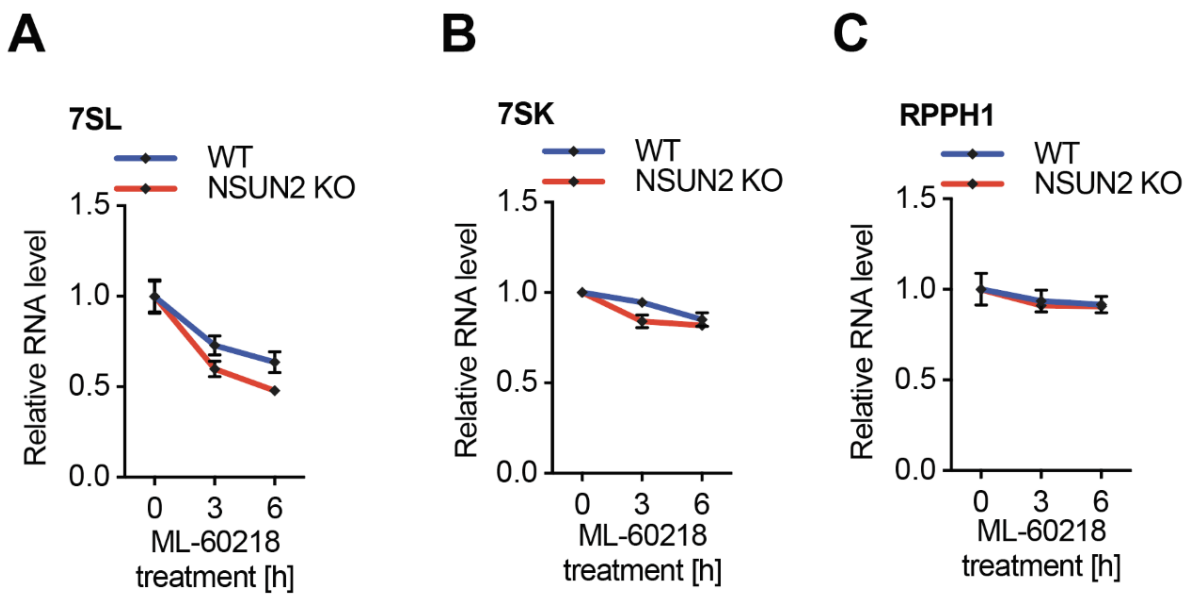

Fig.S10. NSUN2 depletion does not significantly affect the stability of ncRNAs. **A**, Relative RNA levels of 7SL RNA in NSUN2 KO A549 cells *vs*. WT A549 cells. **B**, Relative RNA levels of RPPH1 RNA in NSUN2 KO A549 cells *vs*. WT A549 cells. **C**, Relative RNA levels of 7SK RNA in NSUN2 KO A549 cells *vs*. WT A549 cells. For **A-C**, RT-qPCR quantification was conducted on isolated RNA at time points of 0, 3, and 6 h after incubating the cells with 30 μM of Pol III transcription inhibitor ML-60218. RNA levels were normalized to 0-hour time point in wild-type and NSUN2 KO cells, respectively. Human 18S rRNA level was used as the internal standard for normalization of each time point.

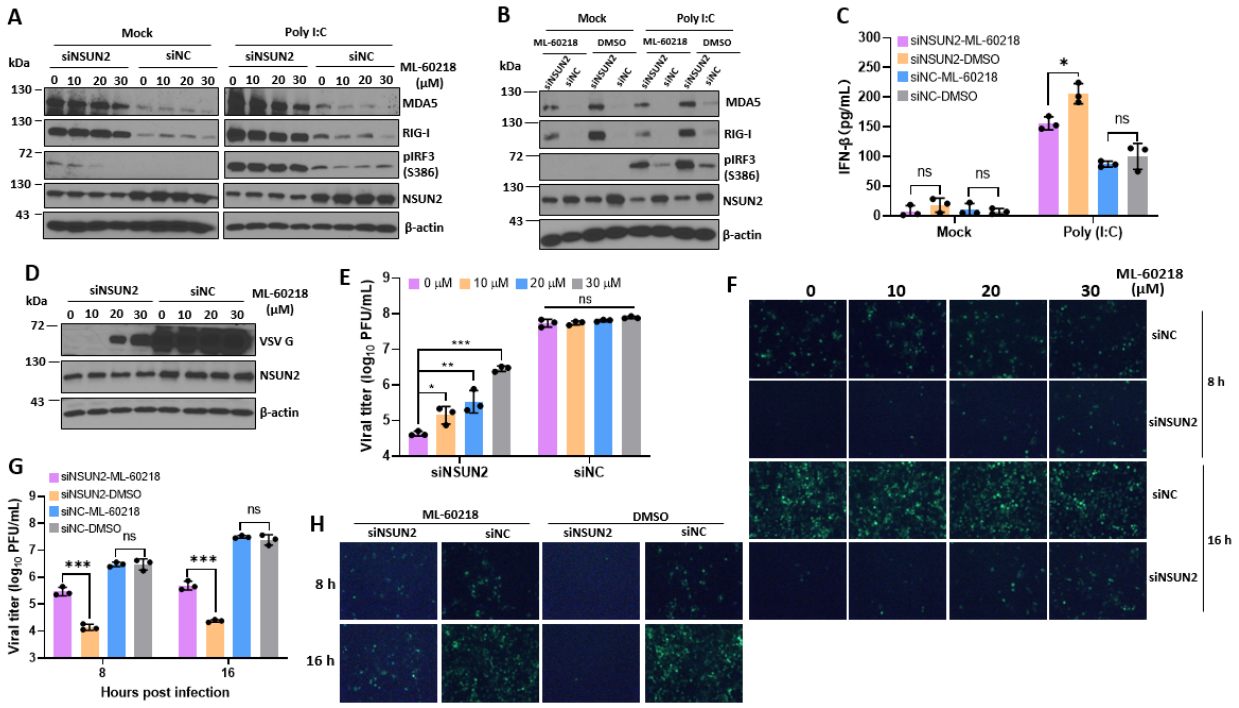

Fig.S11. Inhibition of Pol III transcription partially rescues VSV replication. (A-C) Inhibition of Pol III transcription attenuates IFN signaling. A549 cells were treated with the indicated concentrations of ML-60218 for 10 h and then transfected with siNSUN2 and siNC, and subsequently stimulated with poly I:C. Cell lysates were subjected to Western blot (**A and B**). IFN-β in cell culture supernatants was detected by ELISA (**C**). **(D-H) Inhibition of Pol III transcription partially rescues VSV replication.** A549 cells were treated with increasing doses of ML-60218 for 10 h before transfection with siNSUN2 and siNC, and then infected with rVSV-GFP at an MOI of 0.1 (**D-F**). Cell lysates were prepared for Western blot (**D**) against VSV G, NSUN2, and β-actin, VSV titer (**E**) was determined by plaque assay, and representative GFP images **(F)** were taken by fluorescence microscopy. A549 cells were treated with 30 μM of ML-60218 for 10 h before transfection with siNSUN2 and siNC, and then infected with rVSV-GFP at an MOI of 0.1 (**G-H**). VSV titer (**G**) was determined by plaque assay, and representative GFP images **(H)** were taken by fluorescence microscopy. Data were analyzed using Student's *t*-test (*$P < 0.05$; **$P < 0.01$; and ***$P < 0.001$).

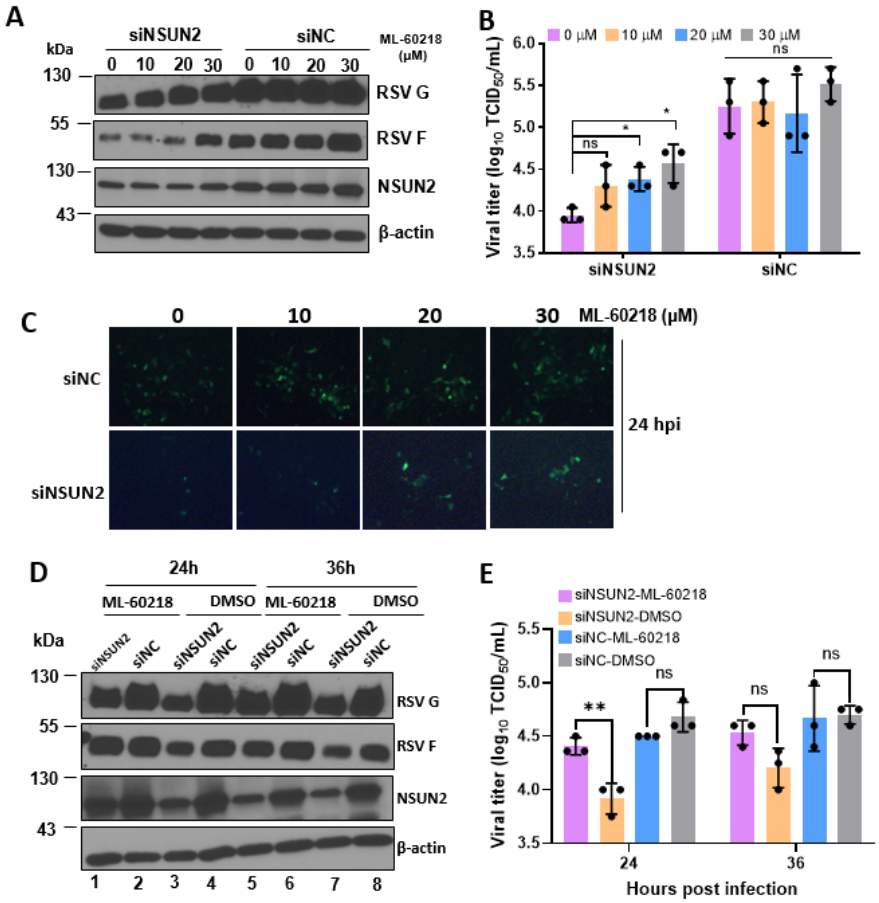

Fig.S12. Inhibition of Pol III transcription partially rescues RSV replication. A549 cells were treated with increasing doses of ML-60218 for 10 h before transfection with siNSUN2 and siNC, and then infected with rgRSV (**A-C**) at an MOI of 0.1. Cell lysates were prepared for Western blot **(A)** against NSUN2, β-actin, and RSV G and F proteins, RSV titer (**B**) was determined by $TCID_{50}$ assay, and representative GFP images (**C**) were taken by fluorescence microscopy. A549 cells were treated with 30μM of ML-60218 for 10 h before transfection with siNSUN2 and siNC, and then infected with rgRSV (**D-E**) at an MOI of 0.1. Cell lysates were prepared for Western blot **(D)** against NSUN2, β-actin, and RSV G and F proteins, RSV titer (**E**) was determined by $TCID_{50}$ assay. Data were analyzed using Student's *t*-test (*$P < 0.05$; and **$P < 0.01$).

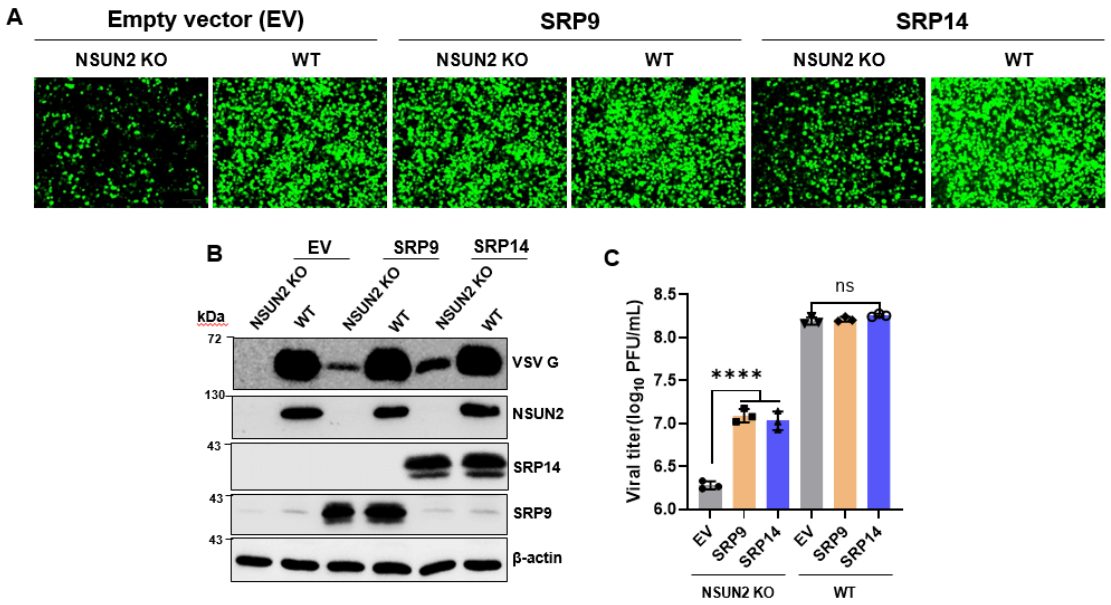

Fig.S13. Overexpression of SRP9 and SRP14 rescues VSV replication and gene expression in NSUN2-KO A549 cells. NUSUN2 knockout A549 cells or control sgRNA A549 cells were transfected with 1 μg of empty vector (EV) or SRP9 and SRP14, followed by infection with rVSV-GFP at an MOI of 0.1. At 18 hpi, GFP images were captured by fluorescence microscopy (**A**), protein expression was determined by Western blot (**B**), and VSV virus titer were determined by plaque assay (**C**).

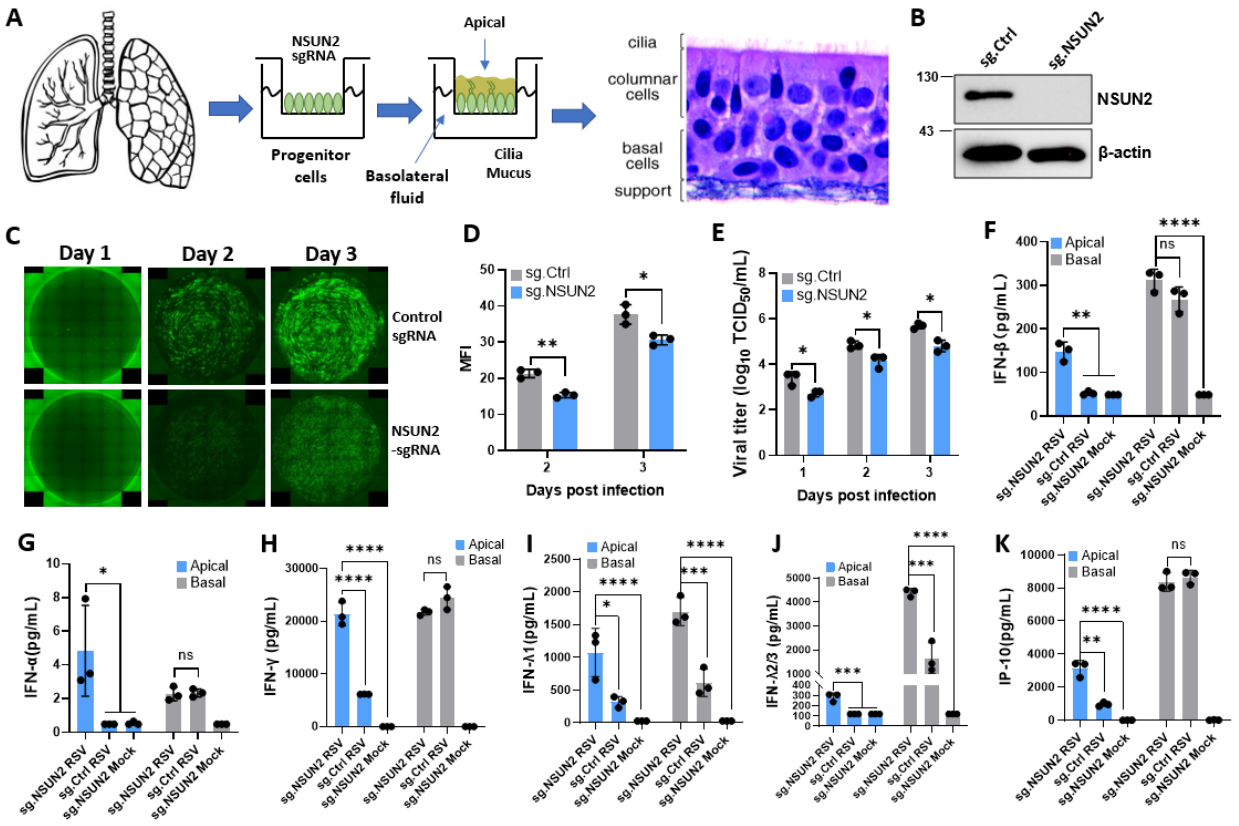

Fig.S14. Knockdown of NSUN2 in HBE culture inhibits RSV replication and enhances the type I IFN response. (A) Diagram describing NSUN2-depletion in HBE cultures. Human lung progenitor cells derived from donor bronchi were seeded on collagen-coated 6.5 mm Transwells and were transduced with lentivirus expressing sgRNA targeting NSUN2 or control sgRNA and were differentiated at the air-liquid interface in the presence of puromycin (2μg/ml) to generate well-differentiated, polarized cultures. **(B) Western blot analysis of NSUN2 in HBE**. At week 4, HBE cultures were lysed by RIPA buffer for Western blot analysis. **(C) Spreading of rgRSVs in HBE culture**. HBE cultures were inoculated with 400 $TCID_{50}$ of rgRSV. At the indicated time, virus spread was monitored by fluorescence microscopy. Representative micrographs at each time point are shown. **(D) Quantification of GFP intensity of digital images using Image J**. **(E) Virus released from rgRSV-infected HBE culture.** At days 1, 2, and 3, apical washes were collected,

and infectious virus was determined by $TCID_{50}$ assay. Viral titers are the geometric mean titer (GMT) of three independent experiments ± standard deviation. (**F-K**) **Enhanced innate immune response after NSUN2 depletion**. The apical washes and basolateral fluids from the rgRSV-infected or mock-infected HBE cultures were collected, and IFN-β (**F**), IFN-α (**G**), IFN-γ (**H**), IFN-λ1 (**I**), IFN-λ2/3 (**J**), IP-10 (**K**) levels were assayed using the Legendplex human antivirus response panel (Biolegend) bead assay. Data were analyzed using the Student's *t*-test and $*P < 0.05$; $**P < 0.01$; $***P < 0.001$; $****P < 0.0001$.

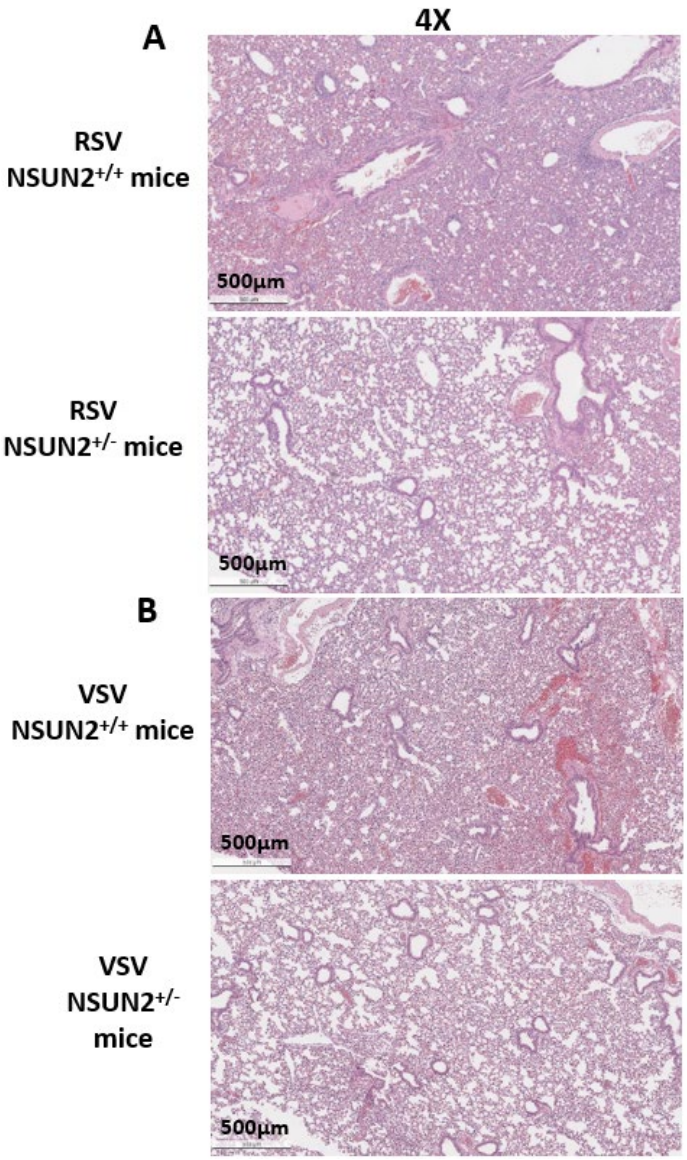

Fig.S15. Knockout of NSUN2 in mice reduces lung pathology after RSV (A) and VSV (B) infection. Representative lung histological images of 4 × magnification from each group were shown. Results showed that lung sections from NSUN2$^{+/-}$ mice had less lung pathology compared to those from WT NSUN2$^{+/+}$ mice.

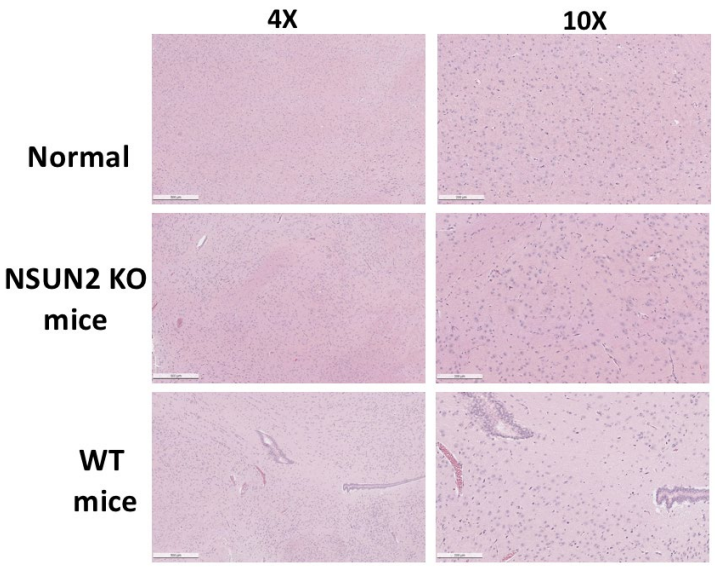

Fig.S16. Brain histology from VSV-infected mice. Brain histology score from VSV-infected mice. Scores were based on the signs of encephalitis such as neuronal necrosis, gliosis, mononuclear cell infiltration, and neuronophagia with lymphocytic perivascular cuffing. Scores: 0, no lesion; 1, mild; 2, moderate; 3, severe.

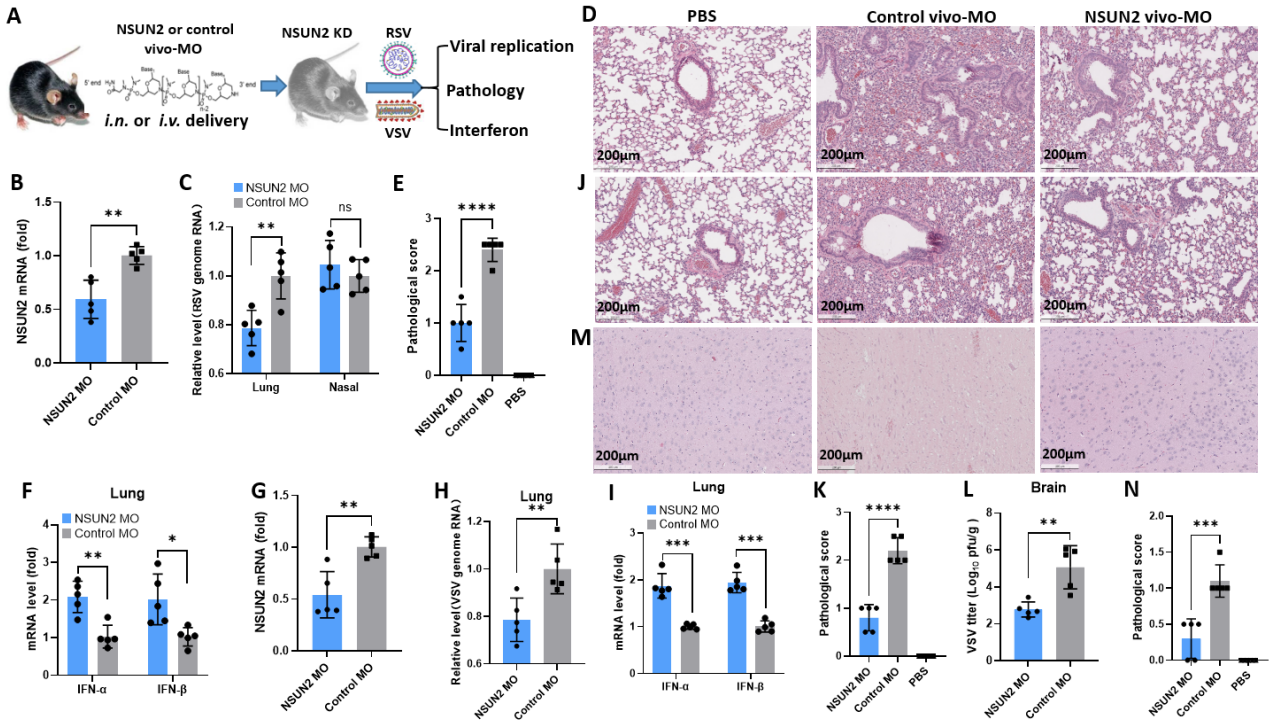

Fig.S17. Knockdown of NSUN2 in mice reduces viral replication and enhances type I IFN responses. (A) A cartoon model for knockdown of NSUN2 in mice using vivo-MO. Vivo-MO were delivered into mice intranasally and intravenously for RSV **(B-F)** and VSV (**G-N**) infection, respectively. **(B) Knockdown of NSUN2 in lung tissues by intranasal delivery of vivo-MO.** NSUN2 mRNA was quantified by real-time RT-PCR. **(C) RSV genome replication in lung and nasal turbinate**. RSV genome RNA was quantified by real-time RT-PCR. **(D) Quantification of IFN-α and IFN-β mRNA in lungs by real-time RT-PCR**. **(E) Lung histology from rgRSV-infected mice.** Sections of lung tissue stained with Hematoxylin-eosin (HE) and imaged by light microscopy. Micrographs with ×10 magnification (scale bar of 200 μm) are shown. **(F) Lung histology score from rgRSV-infected mice**. Each slide was scored based on severity of peribronchiolitis, perivasculitis, bronchiolitis, alveolitis, and interstitial pneumonia. Scores: 0, no lesion; 1, mild; 2, moderate; 3, severe. **(G) Knockdown of NSUN2 in lung tissues by intravenous delivery of vivo-MO. (H) Quantification of RSV genome in lung by real-time RT-PCR. (I)**

Quantification of IFN-α and IFN-β mRNA in lungs by real-time RT-PCR. **(J) Lung histology from VSV-infected mice. (K) Lung histology score from VSV-infected mice**. **(L) Brain histology from VSV-infected mice. (M) Brain histology score from VSV-infected mice**. Scores were based on the severity of encephalitis including neuronal necrosis, gliosis, mononuclear cell infiltration, and neuronophagia with lymphocytic perivascular cuffing. Scores: 0, no lesion; 1, mild; 2, moderate; 3, severe. Data were analyzed using Student's *t*-test and $*P < 0.05$; $**P < 0.01$; $***P < 0.001$; $****P < 0.0001$.

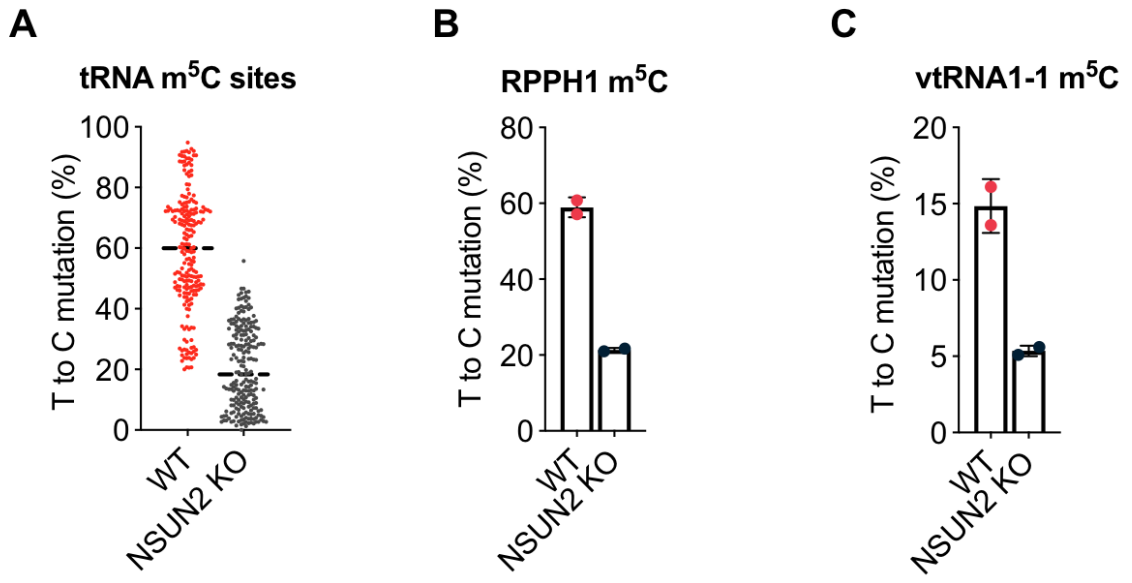

Fig.S18. Knockout of NSUN2 reduces tRNA, RPPH1, and vtRNA m^{5}C methylation in HIV-1-infected THP-1 cells. (**A**) The mutation levels of 224 m^{5}C sites in cytoplasmic tRNAs with and without NSUN2 knockout in HIV-1-infected THP-1 cells. *P* values were determined using Wilcoxon matched-pairs signed rank test for paired samples. *$P < 0.05$; **$P < 0.01$; ***$P < 0.001$; ****$P < 0.0001$. (**B**) The mutation levels of one m^{5}C site in RPPH1 RNA with and without NSUN2 depletion in HIV-1-infected THP-1 cells. (**C**) The mutation levels of one m^{5}C site in vault RNA (vtRNA1-1) from with and without NSUN2 depletion in HIV-1-infected THP-1 cells. For **B**-**C**, Mean values ± SD are shown; $n = 2$.

Interpretation for Fig.S18: We prepared HIV-1 infected NSUN2-KO THP-1 cells and the control cells, followed by isolating rRNA-depleted total RNA for m^{5}C bisulfite sequencing. We primarily analyzed m^{5}C methylated sites in THP-1 host RNAs. We successfully identified the consistent m^{5}C site in RPPH1 RNA (**panel B**), which displayed ~60% and ~20% mutation ratios in WT and NSUN2-depleted THP-1 cells, respectively. Compared with WT A549 cells, the RPPH1 m^{5}C site

shows a higher methylation in WT THP-1 cells. In THP-1 cells, we then confirmed the NSUN2-methylated m^5C site in vault RNA (**Panel C**) and hundreds of NSUN2-methylaterd m^5C sites on cytoplasmic tRNA (**Panel A**).

Table S1: **List of m^{5}C sites in HIV-1 RNA extracted from HIV-1 infected THP-1 cells.**

Virus	Position	Mutation ratio_WT Treated_rep1 %	Mutation ratio_WT Treated_rep2 %	Overlap CEM cellular RNA	Overlap CEM virion RNA
HIV	8	3.33	4.76	No	Yes
HIV	96	2.82	3.90	Yes	Yes
HIV	432	8.33	2.86	Yes	Yes
HIV	773	3.51	2.90	No	Yes
HIV	1095	2.50	3.33	No	Yes
HIV	1209	2.13	3.57	No	Yes
HIV	1210	4.35	3.45	No	Yes
HIV	1295	2.78	3.08	No	Yes
HIV	1426	2.70	2.63	No	Yes
HIV	1833	2.86	3.13	No	No
HIV	1996	2.86	2.27	Yes	Yes
HIV	2478	3.90	2.17	No	Yes
HIV	2589	3.33	5.56	No	Yes
HIV	3002	3.30	2.33	Yes	Yes
HIV	3095	2.70	2.08	Yes	Yes
HIV	3429	2.50	4.23	Yes	Yes
HIV	3459	2.13	3.33	Yes	Yes
HIV	3994	2.13	3.45	No	No
HIV	4014	2.04	2.17	No	No
HIV	4100	3.57	5.00	No	No
HIV	4462	2.50	2.56	Yes	Yes
HIV	4518	2.86	2.74	Yes	Yes
HIV	4820	3.92	2.27	Yes	Yes
HIV	5168	2.04	2.86	Yes	Yes
HIV	5404	2.78	2.04	No	No
HIV	5651	2.44	3.03	No	No
HIV	5833	3.08	3.08	Yes	Yes
HIV	6426	4.76	2.38	Yes	Yes
HIV	6874	2.08	2.17	No	Yes
HIV	7087	2.37	4.32	No	No
HIV	7443	2.00	2.20	No	Yes
HIV	7529	2.21	2.03	Yes	Yes
HIV	7564	3.80	2.23	No	Yes
HIV	9012	3.03	3.57	Yes	Yes
HIV	9028	2.41	3.66	Yes	Yes

Interpretation for Table S1: We investigated the m^{5}C signals on HIV viral RNA in the same sequencing libraries in **Fig.S18**. We identified 35 detectable m^{5}C sites on HIV viral RNA. We then compared these sites with the enriched m^{5}C peaks reported in the data set from Courtney *et al*.

2019 (10). First, 46% of the 35 sites can overlap with their m^5C peaks on HIV viral RNA from CEM cellular total RNA; Second, 80% of the 35 sites can overlap with their m^5C peaks on HIV viral RNA from CEM virion RNA. We found all these 35 m^5C sites in HIV RNA displayed low mutation levels around 2-6%. However, we saw m^5C sites at 20-90% mutation level in RSV genome. There may be two possibilities to explain these results. First, our HIV-1 RNA was prepared from THP-1 cells whereas Courtney *et al*. used RNA extracted from CEM cells (10). Thus, m^5C methylation in different cell lines may be different. Second, the m^5C sequencing method reported by Courtney *et al*. may have a higher detection sensitivity. However, a unique advantage of our bisulfite-based method is that it provides the stoichiometry information of m^5C sites in RNA.

Table S2: The motif sequence context around each m^5C site detected in RSV genome.

Position	m-3	m-2	m-1	M	m+1	m+2	m+3
958	A	T	A	C	T	T	G
962	G	A	T	C	A	T	A
1019	A	T	G	C	A	T	A
3050	T	A	A	C	T	A	A
3085	C	T	T	C	T	G	T
3088	G	G	T	C	T	T	C
3133	T	G	G	C	G	G	A
4032	A	C	A	C	T	G	A
4034	A	C	A	C	A	C	T
4036	T	A	A	C	A	C	A
4098	C	C	A	C	A	G	A
4100	A	A	C	C	A	C	A
4101	G	A	A	C	C	A	C
4965	G	G	T	C	T	T	G
5000	T	T	G	C	T	G	G
5459	T	G	G	C	G	T	G
5463	C	T	A	C	T	G	G
5466	T	A	A	C	T	A	C
8183	G	T	A	C	A	T	A
8339	T	A	A	C	G	A	T

Prediction of m^5C writer proteins that may add m^5C sites to RSV genome. For RSV genome RNA, we identified 20 m^5C sites. Our data suggest that NSUN2 is not responsible for these m^5C methylation (**Fig. S2A**). It is known that m^5C methyltransferase family includes 8 proteins: NSUN1-7 and DNMT2. It is possible that other m^5C methyltransferases may add these m^5C sites on RSV viral RNA. One future experiment is to generate A549 cells lacking each m^5C methyltransferase, followed by RSV infection and m^5C sequencing, which will allow us to identify the specific m^5C methyltransferase responsible for adding m^5C to RSV RNA.

RSV replicates entirely in cytoplasm. m^5C methyltransferases that locate in cytoplasm may have access to RSV RNA. Based on the cellular localization of each m^5C methyltransferase and their motif preference, we speculate that DNMT2 may be responsible for adding m^5C sites in RSV genome. This speculation is based on the below analysis.

In the **Table S2**, we listed the motif context of each m^5C methylated site on RSV viral RNA. It is known that human NSUN1 and NSUN5 are located in the nucleolus and methylate 28S rRNA m^5C4413 and m^5C376, respectively (11). NSUN1 targets GAU(m^5C)CUU motif (12) whereas NSUN5 targets AGC(m^5C)AAA motif (13). Obviously, these two motifs of NSUN1 and NSUN5 are different from the motifs we observed around m^5C sites on RSV viral RNA. NSUN3 locates inside mitochondria and installs m^5C at position 34 of $tRNA^{Met}$, in a motif of GCC(m^5C)AUA (14). NSUN4 also locates inside mitochondria and controls the m^5C methylation at 12S rRNA position 841, in a motif of GCC(m^5C)GUC (15, 16). These two motifs of NSUN3 and NSUN4 are also quite different from the motifs we observed around m^5C sites on RSV viral RNA. Thus, NSUN1, NSUN3, NSUN4 and NSUN5 may not be responsible for methylating RSV RNA based on the motif analysis and their cellular localization.

NSUN7 locates inside cell nucleus and might not work on RSV RNA. NSUN6 and DNMT2 are localized in cytosol which may be the possible 'writer' protein for m^5C methylation on RSV viral RNA. However, NSUN6 shows a very strong motif preference as "(m^5C)UCCA" which seems different from our observations in m^5C methylation on RSV viral RNA(17). Therefore, we speculate that DNMT2 may be the potential m^5C methyltransferase for RSV viral RNA, because it is known to bind and methylate various mRNA species in a sequence-independent manner (18). However, future studies are needed to identify which enzyme is responsible for m^5C methylation of viral RNA.

Table S3: **List of primers for RT-qPCR and RT-PCR**

Primers used for RT-qPCR

	Forward (5'-3')	Reverse (5'-3')
RN7SK	GGGTTGATTCGGCTGATCT	GGGGATGGTCGTCCTCTT
RN7SL	GCTACTCGGGAGGCTGAGGCT	TATTCACAGGCGCGATCC
RPPH1	AGCTTGGAACAGACTCACGG	AATGGGCGGAGGAGAGTAGT
β-actin	GTTTCTCTGCCGGTCGCAAT	ATGGAAGGAAACACGGCTCG
RSV genome /antigenome	AAATGCGTACAACAAACTTGCATAA	AATATTTCCTTTTCCACAACCTTCC
RSV NS1	CAATTCATTGAGTATGATAAAAGTTAGATTACA	AATATTATTATTAGGGCAAATATCACTACTTGTA
RSV G	AGGACCAACGCACCGCTAAG	GTTCTTGATCTGGCTTGTTGCATC
RSV N	GCTAATCATAAATTCACTGGGTTAATAGG	CAATGTTGATTTGAATTTCAGTTGTTAAG
muIFN-α	GACTCATTCTGCAATGACC	CTCCAGACTTCTGCTCTG
muIFN-β	CCCTATGGAGATGACGGAGA	CTGTCTGCTGGTGGAGTTCA
muβ-actin	AGCCATGTACGTAGCCATCC	CTCTCAGCTGTGGTGGTGAA

Primers used for RT-PCR

	Sequence (5'-3')
T7 RN7SL F	TAATACGACTCACTATAGGGGCCGGGCGCGGTGGCG
T7 RN7SL R	AGAGACGGGGTCTCGCTATGTTG
T7 RN7SK F	TAATACGACTCACTATAGGGGGATGTGAGGGCGATC
T7 RN7SK R	AAAAGAAAGGCAGACTGCCAC

Table S4: **Sample information for high-through sequencing in this study**

Experiment	Samples/replicates	Reads#
Duplicates for bisulfite-seq for RNA m^5C detection in total RNA and mRNA from wild-type and NSUN2-knockout A549 cells, under RSV or VSV infection.	m5C_WT_Total-RNA_RSV-infected_Input_1	38858820
	m5C_WT_Total-RNA_RSV-infected_Input_2	47395515
	m5C_NSUN2-KO_Total-RNA_RSV-infected_Input_1	48903514
	m5C_NSUN2-KO_Total-RNA_RSV-infected_Input_2	27980325
	m5C_WT_Total-RNA_VSV-infected_Input_1	22100689
	m5C_WT_Total-RNA_VSV-infected_Input_2	37267693
	m5C_NSUN2-KO_Total-RNA_VSV-infected_Input_1	29995795
	m5C_NSUN2-KO_Total-RNA_VSV-infected_Input_2	31205433
	m5C_WT_Total-RNA_RSV-infected_BS-treated_1	99955699
	m5C_WT_Total-RNA_RSV-infected_BS-treated_2	117533042
	m5C_NSUN2-KO_Total-RNA_RSV-infected_BS-treated_1	110004886
	m5C_NSUN2-KO_Total-RNA_RSV-infected_BS-treated_2	91765440
	m5C_WT_Total-RNA_VSV-infected_BS-treated_1	97546760
	m5C_WT_Total-RNA_VSV-infected_BS-treated_2	62735299
	m5C_NSUN2-KO_Total-RNA_VSV-infected_BS-treated_1	98261811
	m5C_NSUN2-KO_Total-RNA_VSV-infected_BS-treated_2	92045704
	m5C_WT_mRNA_BS-treated_1	17621250
	m5C_WT_mRNA_BS-treated_2	17620225
	m5C_NSUN2-KO_mRNA_BS-treated_1	17272948
	m5C_NSUN2-KO_mRNA_BS-treated_2	17275467
Duplicates for RIP-seq of RIG-I IP-enriched RNA from wild-type and NSUN2-knockout A549 cells, under RSV or VSV infection.	RIG-I_RIP_WT_VSV-infected_Input_1	22988245
	RIG-I_RIP_WT_VSV-infected_Input_2	24592623
	RIG-I_RIP_WT_RSV-infected_Input_1	24096387
	RIG-I_RIP_WT_RSV-infected_Input_2	21384956
	RIG-I_RIP_NSUN2-KO_VSV-infected_Input_1	24635611
	RIG-I_RIP_NSUN2-KO_VSV-infected_Input_2	12124636
	RIG-I_RIP_NSUN2-KO_RSV-infected_Input_1	25308106
	RIG-I_RIP_NSUN2-KO_RSV-infected_Input_2	30017110
	RIG-I_RIP_WT_VSV-infected_IP_1	17804047
	RIG-I_RIP_WT_VSV-infected_IP_2	23166816
	RIG-I_RIP_WT_RSV-infected_IP_1	20056146
	RIG-I_RIP_WT_RSV-infected_IP_2	20553729
	RIG-I_RIP_NSUN2-KO_VSV-infected_IP_1	12236043
	RIG-I_RIP_NSUN2-KO_VSV-infected_IP_2	11808708
	RIG-I_RIP_NSUN2-KO_RSV-infected_IP_1	20209847
	RIG-I_RIP_NSUN2-KO_RSV-infected_IP_2	21677625
Triplicates for RNA-seq of "RNA input" and "anti-dsRNA antibody IP-enriched dsRNA" from wild-type and NSUN2-knockout A549 cells.	dsRNA-seq_WT_Input_1	55219355
	dsRNA-seq_WT_Input_2	52882462
	dsRNA-seq_WT_Input_3	55470948
	dsRNA-seq_WT_IP_1	56159269
	dsRNA-seq_WT_IP_2	59142511
	dsRNA-seq_WT_IP_3	62457237
	dsRNA-seq_NSUN2-KO_Input_1	56164498
	dsRNA-seq_NSUN2-KO_Input_2	50425939
	dsRNA-seq_NSUN2-KO_Input_3	54635215
	dsRNA-seq_NSUN2-KO_IP_1	60396860
	dsRNA-seq_NSUN2-KO_IP_2	64496558
	dsRNA-seq_NSUN2-KO_IP_3	66886048

References

1. S. Blanco *et al.*, The RNA-methyltransferase Misu (NSun2) poises epidermal stem cells to differentiate. *PLoS Genet* **7**, e1002403 (2011).
2. S. Hussain *et al.*, NSun2-Mediated Cytosine-5 Methylation of Vault Noncoding RNA Determines Its Processing into Regulatory Small RNAs. *Cell Rep* **4**, 255-261 (2013).
3. C. Mary *et al.*, Residues in SRP9/14 essential for elongation arrest activity of the signal recognition particle define a positively charged functional domain on one side of the protein. *RNA* **16**, 969-979 (2010).
4. L. S. Zhang *et al.*, ALKBH7-mediated demethylation regulates mitochondrial polycistronic RNA processing. *Nat Cell Biol* **23**, 684-691 (2021).
5. S. M. Johnson *et al.*, Respiratory Syncytial Virus Uses CX3CR1 as a Receptor on Primary Human Airway Epithelial Cultures. *PLoS pathogens* **11**, e1005318 (2015).
6. M. G. Xue *et al.*, Viral RNA N-6-methyladenosine modification modulates both innate and adaptive immune responses of human respiratory syncytial virus. *Plos Pathog* **17** (2021).
7. M. G. Xue *et al.*, Viral N-6-methyladenosine upregulates replication and pathogenesis of human respiratory syncytial virus. *Nat Commun* **10** (2019).
8. M. G. Xue *et al.*, Stable Attenuation of Human Respiratory Syncytial Virus for Live Vaccines by Deletion and Insertion of Amino Acids in the Hinge Region between the mRNA Capping and Methyltransferase Domains of the Large Polymerase Protein. *J Virol* **94** (2020).
9. Y. M. Ma *et al.*, mRNA Cap Methylation Influences Pathogenesis of Vesicular Stomatitis Virus In Vivo. *J Virol* **88**, 2913-2926 (2014).
10. D. G. Courtney *et al.*, Epitranscriptomic Addition of m(5)C to HIV-1 Transcripts Regulates Viral Gene Expression. *Cell Host Microbe* **26**, 217-+ (2019).
11. K. E. Bohnsack, C. Hobartner, M. T. Bohnsack, Eukaryotic 5-methylcytosine (m(5)C) RNA Methyltransferases: Mechanisms, Cellular Functions, and Links to Disease. *Genes (Basel)* **10** (2019).
12. G. Bourgeois *et al.*, Eukaryotic rRNA Modification by Yeast 5-Methylcytosine-Methyltransferases and Human Proliferation-Associated Antigen p120. *Plos One* **10** (2015).
13. M. Schosserer *et al.*, Methylation of ribosomal RNA by NSUN5 is a conserved mechanism modulating organismal lifespan. *Nat Commun* **6** (2015).
14. S. Haag *et al.*, NSUN3 and ABH1 modify the wobble position of mt-tRNAMet to expand codon recognition in mitochondrial translation. *EMBO J* **35**, 2104-2119 (2016).
15. M. D. Metodiev *et al.*, NSUN4 Is a Dual Function Mitochondrial Protein Required for Both Methylation of 12S rRNA and Coordination of Mitoribosomal Assembly. *Plos Genetics* **10** (2014).
16. H. Chen *et al.*, The human mitochondrial 12S rRNA m(4)C methyltransferase METTL15 is required for mitochondrial function. *J Biol Chem* **295**, 8505-8513 (2020).
17. J. Liu *et al.*, Sequence- and structure-selective mRNA m(5)C methylation by NSUN6 in animals. *Natl Sci Rev* **8**, nwaa273 (2021).
18. R. R. Dev *et al.*, Cytosine methylation by DNMT2 facilitates stability and survival of HIV-1 RNA in the host cell during infection. *Biochem J* **474**, 2009-2026 (2017).